ARMY RESEARCH LABORATORY

Small-Caliber Projectile Target Impact Angle Determined from Close Proximity Radiographs

by Tyler E. Ehlers, Bernard J. Guidos, David W. Webb

ARL-TR-3943   **October 2006**

NOTICES

Disclaimers

The findings in this report are not to be construed as an official Department of the Army position, unless so designated by other authorized documents.

Citation of manufacturers' or trade names does not constitute an official endorsement or approval of the use thereof.

DESTRUCTION NOTICE—For classified documents, follow the procedures in DoD 5220.22-M, National Industrial Security Program Operating Manual, Chapter 5, Section 7, or DoD 5200.1-R, Information Security Program Regulation, C6.7. For unclassified, limited documents, destroy by any method that will prevent disclosure of contents or reconstruction of the document.

Army Research Laboratory
Aberdeen Proving Ground, MD 21005-5069

ARL-TR-3943 October 2006

Small-Caliber Projectile Target Impact Angle Determined from Close Proximity Radiographs

Tyler E. Ehlers, Bernard J. Guidos, David W. Webb
Weapons and Materials Research Directorate

REPORT DOCUMENTATION PAGE

1. REPORT DATE *(DD-MM-YYYY)*	2. REPORT TYPE	3. DATES COVERED *(From - To)*
October 2006	Final	Jan 2005 – Jun 2006

4. TITLE AND SUBTITLE	5a. CONTRACT NUMBER
Small-Caliber Projectile Target Impact Angle Determined from Close Proximity Radiographs	NA
	5b. GRANT NUMBER
	5c. PROGRAM ELEMENT NUMBER

6. AUTHOR(S)	5d. PROJECT NUMBER
Tyler E. Ehlers, Bernard J. Guidos, David W. Webb	62.AH80/AH84
	5e. TASK NUMBER
	5f. WORK UNIT NUMBER

7. PERFORMING ORGANIZATION NAME(S) AND ADDRESS(ES)	8. PERFORMING ORGANIZATION REPORT NUMBER
U.S. Army Research Laboratory ATTN: AMSRD-ARL-WM-TC Aberdeen Proving Ground, MD 21005-5069	ARL-TR-3943

9. SPONSORING/MONITORING AGENCY NAME(S) AND ADDRESS(ES)	10. SPONSOR/MONITOR'S ACRONYM(S)
U.S. Army Research Laboratory Aberdeen Proving Ground, MD 21005-5069	
	11. SPONSOR/MONITOR'S REPORT NUMBER(S)

12. DISTRIBUTION/AVAILABILITY STATEMENT
Approved for public release; distribution is unlimited.

13. SUPPLEMENTARY NOTES

14. ABSTRACT

Small-caliber rounds have a yaw cycle of approximately three meters, but the magnitude and initial yaw varies from shot to shot, even when fired from the same gun. This yaw cycle becomes a variable that researchers must consider when looking at the lethality of an individual shot and round type, especially when testing at close ranges where the yaw cycle is high. Four orthogonal radiograph images provided measured pairs of pitch, yaw and their Z-locations, a curve is fitted through all four pair of points using a fundamental Aerodynamic equation. The fitted curve is then carried out a known distance to the target where the curve provides an expected pitch, yaw, and total angle of attack at impact. Upon completion of a significant number of shots, this method can provide an accurate estimate of measurement error.

15. SUBJECT TERMS

small caliber, yaw cycle, fundamental aerodynamic equation, error analysis

16. SECURITY CLASSIFICATION OF:			17. LIMITATION OF ABSTRACT	18. NUMBER OF PAGES	19a. NAME OF RESPONSIBLE PERSON
			SAR	51	Tyler E. Ehlers
a. REPORT	**b. ABSTRACT**	**c. THIS PAGE**			**19b. TELEPHONE NUMBER** *(Include area code)*
U	U	U			410-278-1014

Contents

List of Figures

Acknowledgments

INTENTIONALLY LEFT BLANK.

1. Introduction

For small-caliber projectiles such as the 5.56-millimeter (mm) M855, assessments of terminal ballistic performance versus soft targets are conducted by firing a single round into a ballistic gelatin block. The gelatin block is then dissected and the terminal ballistic quantities of interest are obtained by careful measurements of the projectile's path in the target. The process is repeated for a sufficient number of shots, and the results are compiled to form a terminal ballistic model.

The terminal ballistic quantities of interest are commonly represented by mathematical functions that use target impact angle as an independent variable. The target impact angle is a scalar quantity defined here as the angle between the projectile axis and a line normal to the target impact surface. The quality of the terminal ballistic model is influenced by the accuracy of the measured target impact angle from each experiment. For small-caliber projectiles, accurate determination of the target impact angle requires a consideration of aero-ballistic free-flight motion model parameters and awareness of photographic measurement limitations.

This report presents the methodology recently developed at the U.S. Army Research Laboratory (ARL) to calculate the target impact yaw from data measured from close proximity radiographs (i.e., "x-ray images"). The experimental setup and procedures used to capture the radiograph images are detailed in section 2.1. Section 2.2 covers the step-by-step procedures required to reduce the radiograph images into data points. Going further, these data points are used in section 2.3 where they are fit to the analytical aero-ballistic free-flight model. The aerodynamic fit is then extrapolated from the last radiograph to the target to accurately detail the impact angle of the projectile. Section 3 covers the results of testing using this method, and how the data sets can be manipulated. Section 4 covers a procedure for calculating the error of the determined target impact yaw; additionally the results for recent small-caliber firings are shown and the measurement error is estimated.

2. Experiment and Analysis

2.1 Range Setup

The experimental setup followed the basic principles presented in Zook, et al. (1992) and is illustrated in figure 1. The gun muzzle was positioned between 5 and 7 meters (m) from the gelatin block striking surface at 0° quadrant elevation. Four orthogonal pairs of

radiograph stations were situated to capture images at 0.23-m [9-inch (in.)] intervals up-range from the gel block. The fourth, most down-range radiograph station was situated 0.23 m from the gel block. The 150 keV x-ray film was positioned 0.18 m to the left of the line of fire. The 150 keV x-ray heads were .50 m to the right of the line of fire. Therefore the distance between the x-ray generating tubes and the film was 0.68 m.
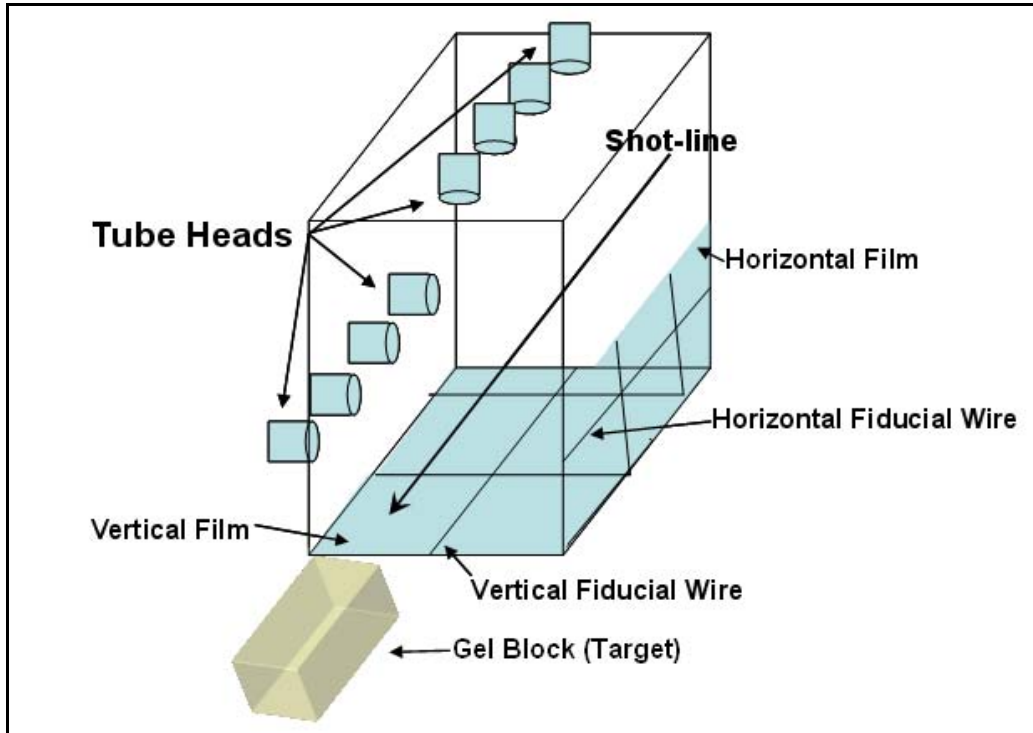
Figure 1. Illustration of experimental setup.

The side tube heads were manually aligned with a level to ensure they were placed on a single plane. The top tube heads were manually aligned with a plumb bob to ensure they were placed on a single plane. If the heads are aligned carefully during this process, the tube heads should be within 2 mm of the intended plane.

Prior to shooting, two 24-gauge wound-steel fiducial wires were suspended. The radiograph films were pressed against the fiducial wires, which serve as reference points. These reference points were later used to calculate projectile angular orientation and lateral position in their respective orthogonal planes. The side-film fiducial wire was positioned horizontally parallel to the boresighted line of fire. These axially aligned wires were manually pulled taut (to an estimated 40-lb tension) and clamped. Because the wire length was only about one meter, it is assumed that no significant catenary droop exists, and no such correction was applied during the subsequent analysis.

For each radiograph film, a wire was suspended perpendicular to the shot line fiducial wires at the same exact downrange location as one of the radiograph heads. These

perpendicular wires detail the location of the head and were subsequently used as reference points when calculating the projectiles downrange location. The system of wires was kept in place for multiple firings. The estimated time delay for each station was programmed into a data acquisition system, the projectile was launched, break screens initiated the time delay generators, and radiographs were obtained of the in-flight projectile and the fiducial wires.

2.2 Radiograph Data Reduction

A total of four 11 in. × 17 in. radiograph films are obtained, each having two images of the projectile, as shown in figure 2. The eight projectile images are measured using a light table and computer digitization software. These measurements are then processed to yield projectile location and angular orientation relative to the line of fire at the four orthogonal stations.
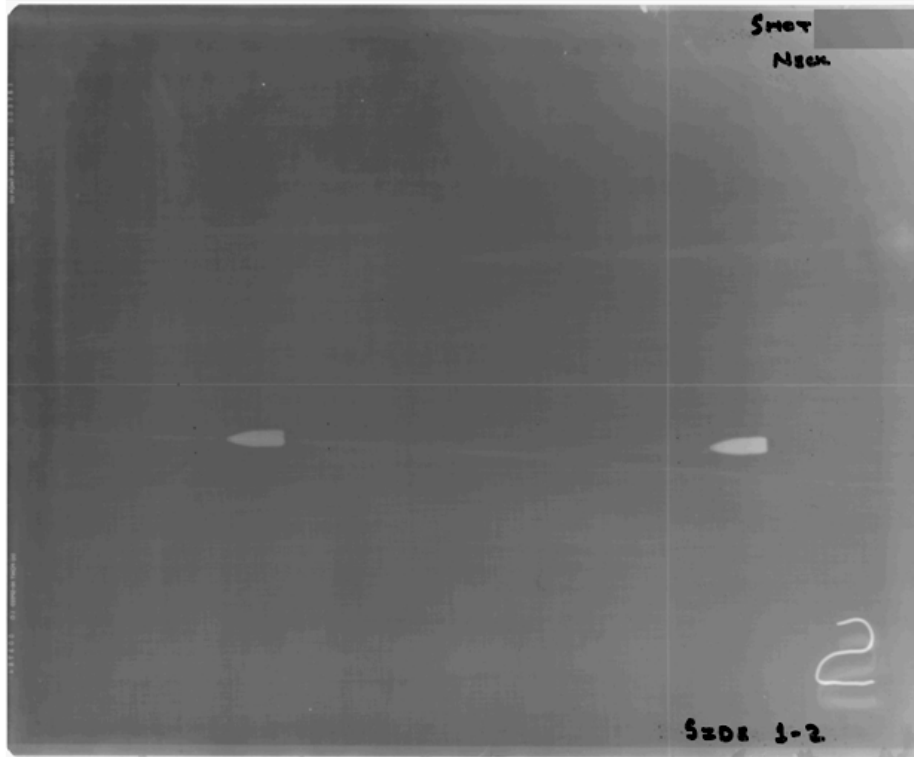
Figure 2. Example of radiograph of M855 projectile.

For small-caliber projectiles, a geometry measurement template can improve the speed and accuracy of the manual digitization process. The template consists of a transparency having concentric images and reference points of the projectile at various incidence in the operator's field of view. These images then have a template laid over them to accurately align the orientation of the bullet and place reference points on the film. These reference

points are located on the corners of the box in figure 3, and are centered over the center of gravity (c.g.) of the bullet.
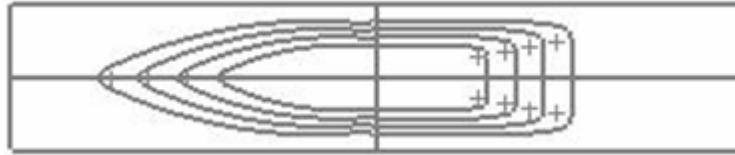
Figure 3. Projectile geometry template.

The specific digitizing process is as follows. A single piece of film is placed on a light table with the bullet flying right to left. Using a light table and Visual Basic® digitizing program, the user takes measurements of the locations of the fiducial wires, a fixed point on the bullet, and the four reference points, which the user must digitize in the following order. The first mark is the crossing of the fiducial wires on the right-hand side of the film. The second mark is located where the user can accurately place the cursor on the extreme left side of the fiducial wire. The third mark is the tip of the bullet of the first flash which is the right image. The fourth through seventh marks, marks made using the template, are the top left reference mark, followed by the bottom left reference mark, followed by the top right mark, concluding with the bottom right. The second image is digitized in the same manner as the first bullet image. The entire process is repeated for each projectile image. The Visual Basic® program outputs the measurements to an Excel® spreadsheet.

These raw measurements are input into the digitizing Excel® program, shown in figures 5 and 6, which calculates the projectile angular orientation. The angle in the vertical plane (i.e., nose pointed up or down) is the pitch angle α. The angle in the horizontal plane (i.e., nose pointed right or left) is the yaw angle β. The total angle of attack is γ. The program calculates the magnification factor, also referred to as K-factor, so the actual location of the bullet when the image was captured can be found. This program also calculates the trajectory angle, i.e., the angle that the projectile is traveling in relation to the axial fiducial wires. The trajectory angle component (i.e., the angle between the projectile velocity vector and the fiducial wire) in the vertical plane is denoted η_α and the trajectory angle component in the horizontal plane is denoted η_β.

The fiducial wires are digitized and used as the reference plane. Because the fiducial wires set the reference plane, the radiograph can be positioned on the light table at any angle. The projectile's reference points are digitized to locate the centerline of the bullet and coordinates of the image. For both orthogonal views, the angle of the bullet relative to the fiducial wire is found for each image using the bullet centerline and the fiducial wire. The angle of the bullet relative to the fiducial wire is referred to here as the apparent angle. The apparent projectile pitch angle, α_A, is determined from the side film;

4

the apparent yaw angle, β_A, is determined from the bottom film. The sign conventions used for pitch and yaw angles are positive nose up and to the right.

To calculate the velocity and the actual location of the projectile, the magnification factor must be determined. The derivation of the magnification factor is given in Zook, et al. (1992, section 5.1); the pertinent equation is restated here:

$$MagnificationFactor = \frac{d_{HFO}(d_{HF} - d_{FF}) - (d_{HFO} - d_{FFO})(l_{AO} - d_{FFO})}{(d_{HFO}d_{HF}) - (l_{AO} - d_{FFO})(l_A - d_{FF})}.$$

Where:

    d_{HF} is the distance from the head to the film,

    d_{HFO} is the distance from the head to the film in the orthogonal view,

    d_{FF} is the distance from the fiducial wire to the film,

    d_{FFO} is the distance from the fiducial wire to the film in the orthogonal view,

    l_A is the apparent location,

    l_{AO} is the apparent location in the orthogonal view.
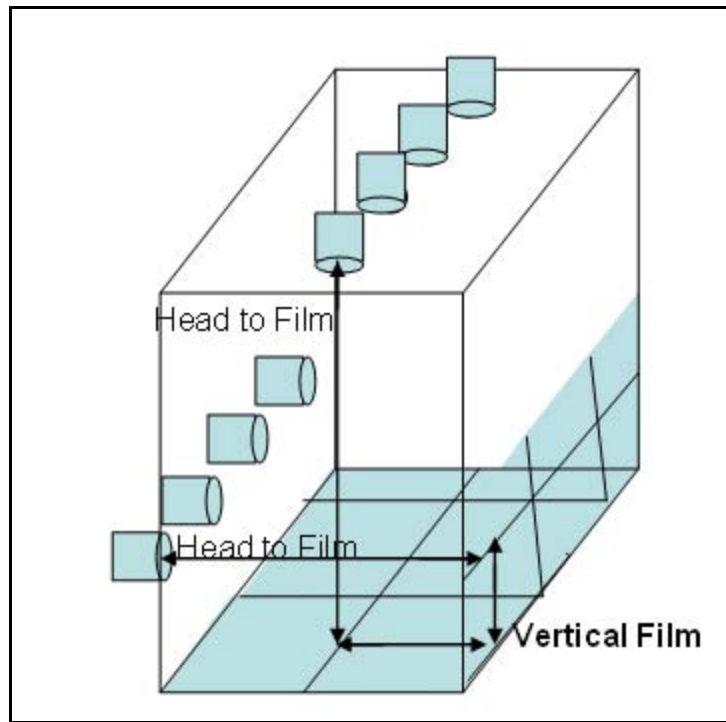
Figure 4. Magnification factor stand.

In order to model the projectile angular motion, the pitch and yaw angles relative to the velocity vector, denoted α and β, respectively, are needed. They are obtained by correcting α_A and β_A by the trajectory angles in both orthogonal planes, η_α and η_β, respectively. The values of η_α and η_β are calculated by taking a linear least squares fit of

the projectile c.g. lateral location at each of the four radiograph stations as a function of range.

The values of η_α and η_β are assumed constant over the flight interval of interest. Linear aerodynamic theory demonstrates that the projectile trajectory experiences an epicyclical (or corkscrew-like) motion, referred to as the swerving motion (e.g., McCoy, 1998). The trajectory angle components, η_α and η_β, vary in a fluctuating manner with respect to range. The magnitude of the fluctuation in each plane is easily calculated using linear aerodynamic theory, and, for the parameters and conditions of this study, is insignificant.

For small angles of attack, the total angle of attack can be approximated as:

$$\gamma = \sqrt{\alpha^2 + \beta^2} . \tag{1}$$

When testing small-caliber ammunition, as α and β are often greater than 2 degrees (deg), the above approximation loses accuracy. In the present study, the following exact relationship is used:

$$\gamma = \tan^{-1}(\sqrt{\tan^2\alpha + \tan^2\beta} . \tag{2}$$

Input Values			Range Values / Rotated Values					
Side Film 1-2			Head Sep	9				
Dig X	**Dig Y**		Shotline to film Side	7.5				
37.875	5.55		Head to Film Side	26.5				
26.573	5.563							
38.341	4.037	Fixed Pt	Head Sep	9				
38.076	4.283		Shotline to film Top	6.63				
38.061	3.827		Head to Film Top	27.75				
40.522	4.166			Image 1	Image 2			
40.509	3.714		K Factor Side	0.70208	0.699238			
29.32	4.179	Fixed Pt	K Factor Top	0.79953	0.795794			
29.047	4.415							
29.031	3.96		PHI Side Film	-0.0659				
31.5	4.323		PHI Bottom Film	-0.3318				
31.487	3.867	Fill to here	**Relative to Origin**				**Rotated**	
				Flash 1 Z	Flash 1 Y		Flash 1 Z	Flash 1 Y
			Fixed Point	0.466	-1.513		-0.46774	-1.512462988
Bottom Film1-2			1	0.201	-1.267		-0.20246	-1.266767964
Dig X	**Dig Y**		2	0.186	-1.723		-0.18798	-1.722784916
38.19	4.764		3	2.647	-1.384		-2.64859	-1.380954404
26.967	4.829		4	2.634	-1.836		-2.63611	-1.832969058
38.665	5.255							
38.296	5.483			Flash 2 Z	Flash 2 Y		Flash 2 Z	Flash 2 Y
38.302	5.029		Fixed Point	0.445	-1.371		-0.44658	-1.370487237
40.744	5.488		1	0.172	-1.135		-0.17331	-1.134801408
40.751	5.031		2	0.156	-1.59		-0.15783	-1.589819511
29.686	5.352		3	2.625	-1.227		-2.62641	-1.223979813
29.3	5.581		4	2.612	-1.683		-2.61393	-1.679994465
29.3	5.126							
31.751	5.562							
31.751	5.108	Fill to here						

Figure 5. Digitizing program digitized points and intermediate calculated values.

Flash Time (us.)	291.1		
Fixed Point Velocity	2580.941229		
Alpha 1	2.199506024	Eta 1-2 Side	0.666207
Beta 1	-0.630876931	Eta 2-3 Side	0.504737
Gamma 1	2.288023385	Eta 3-4 Side	0.077283
Eta Side	0.416202278	Eta 1-4 Side	0.416583
Alpha 2	1.671460884	AVG Eta Side	0.416202
Beta 2	-0.116518858		
Gamma 2	1.675512677	Eta 1-2 Bottom	0.42619
Eta Bottom	0.217140746	Eta 2-3 Bottom	-0.19179
		Eta 3-4 Bottom	0.413907
Fixed Point Location Flash 1	-0.328393006	Eta 1-4 Bottom	0.220258
Fixed Point Location Flash 2	-0.313534567	AVG Eta Bottom	0.217141

Figure 6. Digitizing program output.

At this point the data has been reduced to α, β, and γ in four different locations, those four locations in three dimensional space, and the velocity of the projectile.

2.3 Projectile Motion

The target impact angle is determined from a mathematical fit of the discrete data measured in the radiographs to the linear aerodynamic free-flight equations of motion as outlined by McCoy (1998). The complex angle of attack relative to the flight path is defined as:

$$\tilde{\xi} = \alpha + i\beta, \tag{3}$$

with the pitch angle α being positive for nose up and the yaw angle β being positive for nose right from the gunner's perspective.

The projectile is assumed to be symmetric, spinning, and in flat fire. The modeled trajectory length is assumed to be of low angle of attack and short enough to neglect damping. Under these assumptions, the behavior of the complex angle of attack is given in "modal form" by:

$$\tilde{\xi} = K_F e^{i\phi_{Fo}} e^{i\phi'_F (x-x_0)} + K_S e^{i\phi_{So}} e^{i\phi'_S (x-x_0)}, \tag{4}$$

in which x is the distance along the trajectory, x_0 is the reference location, and the modal parameters are defined as follows:

7

K_F = magnitude of the fast epicyclic modal arm, real and positive,

K_S = magnitude of the slow epicyclic modal arm, real and positive,

ϕ_{Fo} = reference phase angle of the fast epicyclic modal arm, evaluated at $x = x_0$ and real,

ϕ_{So} = reference phase angle of the slow epicyclic modal arm, evaluated at $x = x_0$ and real,

ϕ_F' = turning rate of the fast epicyclic modal arm, real,

ϕ_S' = turning rate of the slow epicyclic modal arm, real.

As viewed from an onlooker standing at the muzzle, the angular motion looks like the nose of the projectile was etching a circular motion; the slow arm, while simultaneously etching another circular motion about that circular motion; the fast arm. Figure 7 depicts this motion. As the bullet travels away, both arms turn in a clockwise motion as the projectile spins in a clockwise direction**.**
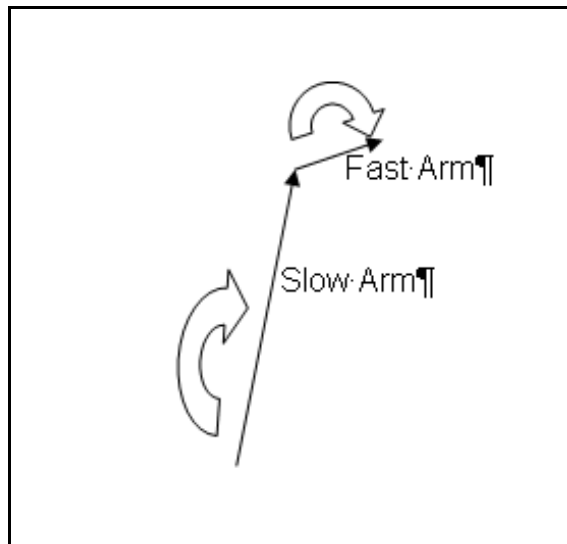
Figure 7. Fast and slow epicyclic modal arms.

Figure 8 depicts the motion of the tip throughout a half of the slow arm cycle.
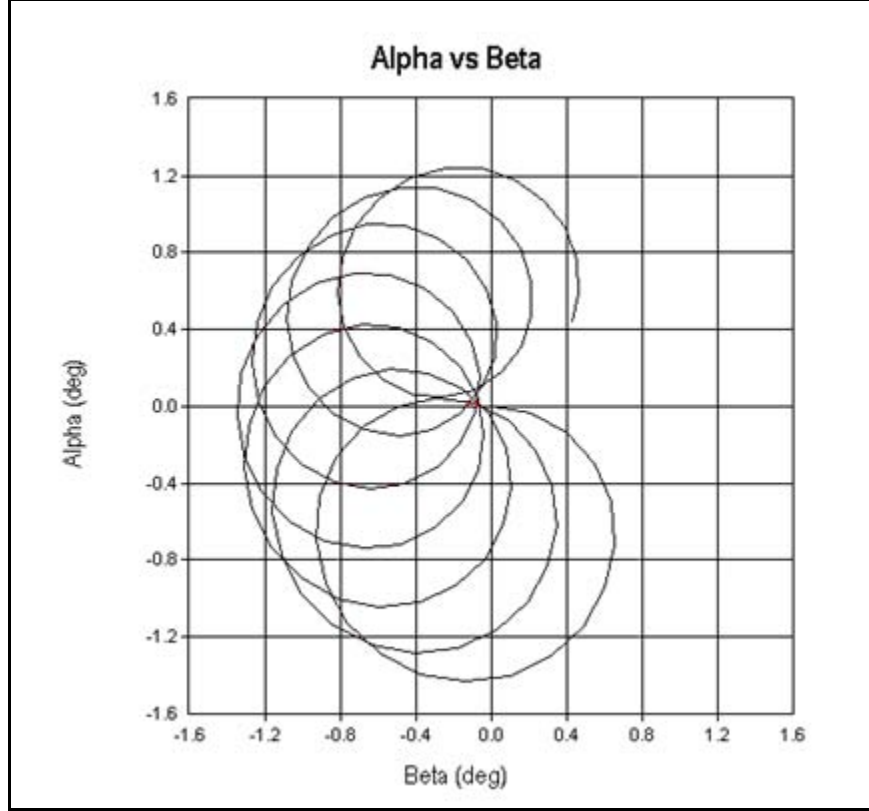
Figure 8. 6-DOF simulation of M855 pitch angle vs. yaw angle.

The pitch and yaw angles can be expressed separately as:

$$\alpha = K_F \cos\left[\phi_{Fo} + \phi'_F (x - x_0)\right] + K_S \cos\left[\phi_{So} + \phi'_S (x - x_0)\right] \tag{5}$$

$$\beta = K_F \sin\left[\phi_{Fo} + \phi'_F (x - x_0)\right] + K_S \sin\left[\phi_{So} + \phi'_S (x - x_0)\right]. \tag{6}$$

For a single shot, digitization and reduction of the radiographs produces the following known quantities: $x_i, \alpha_i, \beta_i,$ for $i = 1...n,$ in which the subscript i is the ith radiograph station out of n total stations. The reference location x_0 is taken as the midpoint of the trajectory encompassed by the radiographs. The six unknown variables are the modal parameters: $K_F, K_S, \phi_{Fo}, \phi_{So}, \phi'_F,$ and ϕ'_S.

The turning rates, ϕ'_F and ϕ'_S, are a function of the projectile's physical properties, spin rate, velocity, atmospheric conditions, and the aerodynamic pitching moment coefficient ($C_{M\alpha}$). The pitching moment coefficient is a measure of the aerodynamic moment in the plane of the instantaneous angle of attack. For the M855 class of ammunition, $C_{M\alpha}$ is positive, indicating that spin is required to stabilize the bullet in flight. The values of ϕ'_F and ϕ'_S (and thus $C_{M\alpha}$) have traditionally been determined from spark range

9

experimentation, which uses spark shadowgraph imagery to provide discrete motion data that can be numerically modeled using linear aerodynamic theory or 6-degrees-of-freedom equations of motion. The values of ϕ'_F and ϕ'_S cannot be accurately obtained from the four radiograph stations used in the present study because the trajectory length is too short and the number of stations is too small. Instead, it is assumed that the turning rates have already been accurately determined. By prescribing the turning rates, the number of unknown variables for each shot is reduced to four: K_F, K_S, ϕ_{Fo}, and ϕ_{So}.

When fitting equations 5 and 6 to the experimental data, it is necessary to specify realistic initial values for the four parameters to be fitted. In this study, the fitting procedure was incorporated into a spreadsheet that included a graph of α versus β, to facilitate the specification of initial values and verify the integrity of the fitted parameters. The four radiograph stations encompassed approximately ⅓ of a fast mode cycle length, so the slow mode magnitude and orientation were easy to visualize as the center of a nearly circular pattern comprised of the four data points. As such, it was convenient to specify the center of this circular pattern using reference pitch and yaw angles, denoted α_{cen} and β_{cen}, rather than specifying K_S and ϕ_{So}. The trigonometric relationships are:

$$K_S = \sqrt{\alpha_{cen}^2 + \beta_{cen}^2} \tag{7}$$

$$\phi_{S_o} = tan^{-1}\frac{\alpha_{cen}}{\beta_{cen}}. \tag{8}$$

An iterative technique is used to fit equations 5 and 6 to the experimental data. The technique determines the values of the four unknown variables by minimizing the root-mean-square (RMS) error of the fit. The RMS error of the fit is defined as:

$$RMS = \sqrt{\sum_{i=1}^{n}\varepsilon_{\alpha_i} + \sum_{i=1}^{n}\varepsilon_{\beta_i}}, \tag{9}$$

in which

$$\varepsilon_{\alpha_i} = \alpha_i - \alpha(x_i) \tag{10}$$

$$\varepsilon_{\beta_i} = \beta_i - \beta(x_i). \tag{11}$$

In these above expressions, α_i and β_i are the values of pitch angle and yaw angle determined from the ith radiograph, and $\alpha(x_i)$ and $\beta(x_i)$ are the values of pitch angle and yaw angle determined from the fitted parameters and evaluated at x_i, the location of the ith radiograph.

After the four fitted parameters are determined, the modeled pitch and yaw angles at the target, α_T and β_T, are calculated by substituting the values back into equations 5 and 6 and solving at x_T. The impact angle of the projectile at the target, γ_T, is found from the equation:

$$\gamma_T = \tan^{-1} \sqrt{\tan^2 \alpha_T + \tan^2 \beta_T} \ . \tag{12}$$

In practice, the user imports the calculated in-flight values from the digitizing program into the Gamma at Impact Prediction Excel® Spreadsheet shown in figure 9. The Gamma at Impact Spreadsheet uses the linear aerodynamics model, equations 5 and 6, to calculate α_T and β_T which are used to calculate the γ_T. The six modal parameters are compiled in the right-most column.

Shot #	Vel 1 (fps)	Vel 2 (fps)	Alpha 1	Beta 1	Gamma 1	Eta 1	Alpha 2	Beta 2	Gamma 2	Eta 2	Alpha 3	Beta 3	Gamma 3	Eta 3
21	2978.2654	2948	1.16	-1.70	2.06	0.52	0.16	-0.10	0.19	-0.18	-1.77	-0.51	1.84	0.52

	X-Ray Stations		X-Ray Data			Analytical Fit			RMS Errors			Modal Parameters	
	X	X	Alpha	Beta	Gamma	Alpha	Beta	Gamma	Alpha	Beta	Gamma	phi'f (deg/m)	211
	(in)	(m)	(deg)	(deg)	(deg)	(deg)	(deg)	(deg)	(deg)	(deg)	(deg)	phi's (deg/m)	30
X-Ray 1	-1	-0.01	1.16	-1.70	2.06	1.15	-1.65	2.02	-0.01	0.05	-0.04	X0 (m)	0.32
X-Ray 2	8	0.21	0.16	-0.10	0.19	0.08	-0.24	0.25	-0.08	-0.14	0.06	Kfast (deg)	2.60
X-Ray 3	17	0.43	-1.77	-0.51	1.84	-1.64	-0.26	1.66	0.12	0.25	-0.17	phif_0 (deg)	88
X-Ray 4	26	0.65	-2.79	-1.64	3.24	-2.81	-1.79	3.33	-0.02	-0.15	0.10	Beta_center	-2.64
Target	36	0.91	0.00			-2.18	-4.23	4.75	0.07	0.16	0.11	Alpha_center	-0.88
				Data Dropin	2948	-2.18	-4.23	4.75	0.1253			Kslow (deg)	2.78
												phis_0 (deg)	-108

Calculated RMS Error

Figure 9: Gamma at Impact Prediction Excel® Spreadsheet.

To run the iterative error reducing program:
      1) Click **Tools** >**Add-Ins** >**Solver.**

The Solver will then be available to open.
      2) Click **Tools** >**Solver.**

The Solver will issue a menu box.

      3) Select the **Target Cell** equal to the calculated **RMS Error** (pointed out in figure 9).

      4) Set the **Equal To** box to **Minimize.**

Set the By **Changing Cells** to contain the cells containing the values of **Kfast**, **phif_0**, **Alpha_center**, and **Beta_center**.

3. Results

The fitted results shown in the spreadsheet of figure 9 were obtained by prescribing the values of the fast arm turning rate, ϕ'_F , to be 211 degrees per meter (deg/m), and the slow arm turning rate, ϕ'_S , to be 30 deg/m. These values were obtained from the spark range results reported by McCoy (1985) and verified by more recent unpublished in-house spark range firings.

Figure 10 shows a typical result of the measured pitch angle versus yaw angle, comparing the actual data to the modeled motion data. The four radiographs encompass approximately ⅓ of a fast mode cycle length. The extrapolated target impact values are also plotted, and located approximately ½ of a fast mode cycle downrange from the first radiograph station. Figure 11 shows the same data plotted versus range, illustrating the sinusoidal-like motion of the projectile in the pitch and yaw planes.
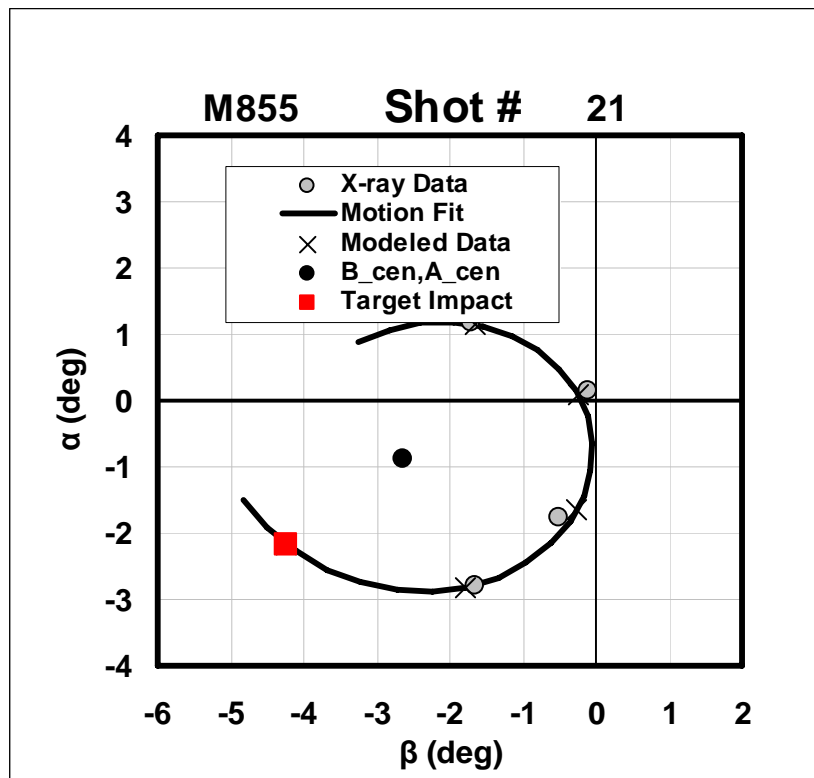
Figure 10. Measured and fitted pitch angle vs. yaw angle.
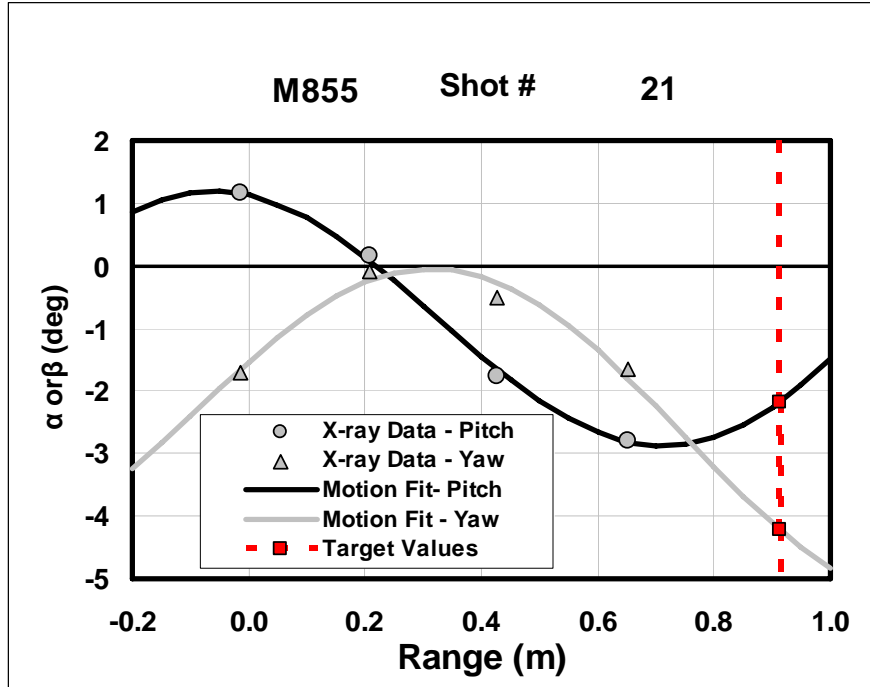
Figure 11. Measured and fitted pitch and yaw angle for shot 21.

Figure 12 shows the measured total angle, comparing the actual data to the modeled motion data. The extrapolated value at the target, γ_T, is apparent in this view. This figure illustrates that using a linear fit of total angle obtained from the radiograph data has the potential to be highly inaccurate. Accurate determination of target impact angle using a linear fit of total angle would require the stations to be clustered extremely close to the target. The approach may be unfeasible considering that the current positioning of radiograph equipment already uses the available space.
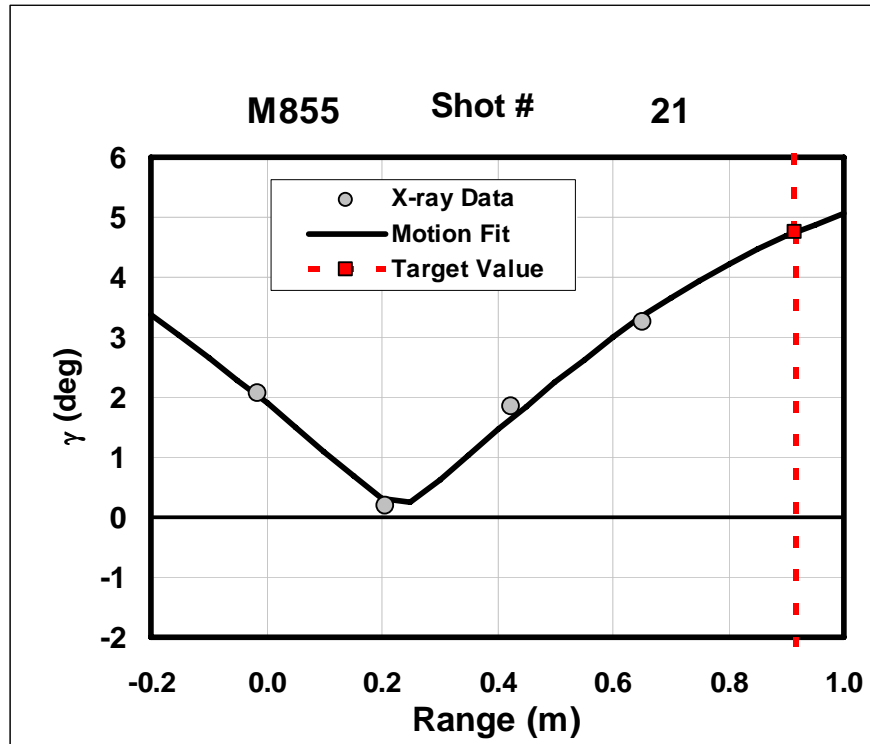
Figure 12. Measured and calculated total impact angle for shot 21.

Figure 13 shows the target impact yaw for 101 shots of the M855 projectile from the same barrel. The result is presented as a distribution from 0 to 5 deg in 0.5 deg increments. For the relative muzzle and target positions used for these firings, the most common range of total impact angle values was 1.0 to 1.5 deg (25 occurrences). The second most common range was 0.5 to 1.0 deg (20 occurrences). Considering that the range 0 to 0.5 deg had 11 occurrences, 56 of 101 shots had impact angles less than 2 deg. The largest total impact angle observed during the firings was between 5.0 and 5.5 deg, with one occurrence. This series of data shows how a data set can be manipulated by repositioning the gun barrel to capture the range of yaws that are commonly found in CQB environments.
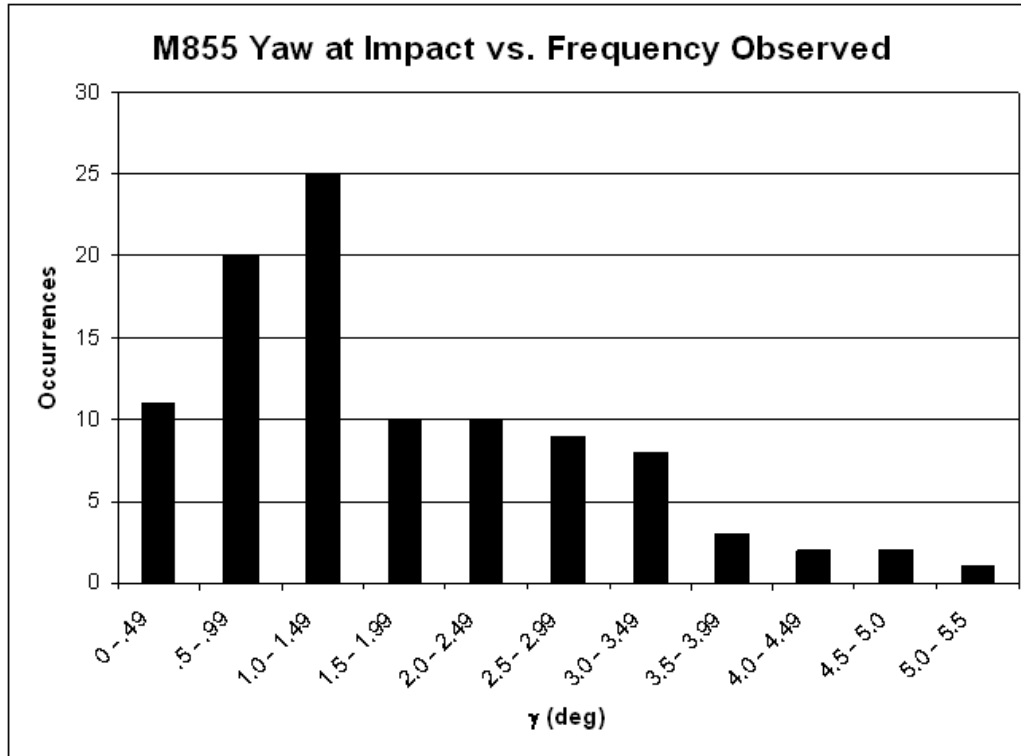
Figure 13. Distribution of measured impact yaw occurrences, M855, 101 shots.

By monitoring the development of the impact angle distribution during a firing program, the distribution of target impact angle occurrences could be tailored for specific purposes. Such tailoring might be desirable; for example, to obtain more occurrences of yaw levels greater than 2 deg in order to more accurately characterize the terminal ballistics in that regime. The tailoring could be achieved by adjusting the distance between the muzzle and the target, using the total yaw behavior illustrated in figure 12 as observed for a large sample of shots. Concurrently, usable estimates of desired muzzle-to-target separation distance that minimizes or maximizes the target impact angle could be achieved using the turning rates of the projectiles.

As an illustrative example, suppose the experimentalist completed the fit from shot 21, figures 10, 11, and 12, and wanted to capture the minimum yaw on shot 22. Figures 11 or 12 indicate that by repositioning the muzzle 0.68 m closer to the target (shifting the fit to the right on the graph) for shot 22, the projectile will be more likely to impact the target during a portion of its yaw cycle where minimum values occur. On the other hand, suppose the experimentalist wanted to capture the maximum yaw on shot 22. By repositioning the muzzle 0.17 m farther from the target (shifting the fit to the left on the graph) for shot 22, the projectile will be more likely to impact the target during a portion of its yaw cycle where maximum values occur.

15

The length of the yaw cycle can be calculated by taking the inverse of the turning rate and multiplying it by one revolution. For example, the M855 fast mode turning rate is 211 deg/m; taking 1/211 m/deg and multiplying it by 360 deg determines that the yaw cycle is 1.7 m. Therefore, minimum impact angles can be expected to occur for muzzle-to-target separation distances of 1.7 m, 3.4 m, 5.1 m, etc.; while maximum impact angles can be expected to occur for muzzle-to-target separation distances of 2.5 m, 4.2 m, 5.9 m, etc.

Another useful total angle distribution that could be extracted from this approach is the maximum angle distribution. Using the linear aerodynamics motion theory, the local maximum angle of attack for an individual shot is the sum of the fast and slow mode arms, $K_F + K_S$. By compiling these values for a set of shots concurrently with the target impact angle, additional characterization of fleet yaw can be generated. Such additional information could not be obtained without a data set that is conducive to linear aerodynamics motion modeling.

4. Error Estimation

An analysis was undertaken to estimate the accuracy of the target impact angle, γ_T, obtained for the experiments in the current study. Two aspects of the error estimation were considered. First, the errors of the trajectory angles, η_α and η_β, as determined from the linear regression fits of the projectile lateral displacements at the four radiograph stations, were estimated. Second, the error of the target impact angle, γ_T, as determined from the linear aerodynamics motion fit of the pitch and yaw data, was estimated. In each case, a statistical analysis of the actual RMS values from the set of shots was compared to the distribution of RMS values from Monte Carlo simulations. The comparison of RMS errors allowed a determination to be made of the expected measurement errors, which are related to the errors of the quantities of interest.

4.1 Trajectory Angle Error

The trajectory angles η_α and η_β, for each shot, were determined via a linear regression of the projectile c.g. lateral displacements as measured at the four radiograph stations. The RMS values of the fits, $R_1, R_2, \ldots, R_N$, are calculated as $R_i = \sqrt{\frac{1}{4} \sum_{j=1}^{4} \left(d_{ij} - \hat{d}_{ij} \right)^2}$, where d_{ij} is the displacement of the ith projectile at the jth station, and $\hat{d}_{ij}$ is its lateral displacement error produced by the least squares fit of the displacement-range pairings measured at the four stations. A frequency histogram was generated from 421 shots, showing the relative number of occurrences of ranges of RMS values as a function of

RMS levels. A statistical analysis was then initiated to reproduce this histogram via simulation in order to relate the RMS histogram to displacement measurement error, and subsequently to trajectory angle error.

The statistical analysis was performed as follows. It can be shown (see appendix A) that the maximum likelihood estimator for the displacement standard deviation, denoted by σ, is $\hat{\sigma} = \sqrt{\dfrac{2}{N}\sum_{i=1}^{N} R_i^{\,2}}$. For the horizontal RMS values from the actual firings, we obtain a standard deviation estimate of $\hat{\sigma}_H = 1.31$ mm; while in the vertical direction, we have $\hat{\sigma}_V = 1.21$ mm.

To verify that the model used to develop this estimate of the displacement standard deviation is tenable, we compare in figure 14 the relative frequency histogram of 421 horizontal RMS values from the actual firings with that of 500,000 simulated RMS values, whose distribution is Weibull[1] with a fixed scale parameter $\dfrac{\hat{\sigma}_H}{\sqrt{2}} = .9255$ mm and shape parameter 2. Figure 15 is a similar comparison for the vertical RMS values.

Figure 14. Comparison of relative frequency histograms of experimental RMS and simulated RMS under assumption of constant errors in the horizontal direction.

---

[1] Several parameterizations exist for the two-parameter Weibull distribution. Compare Mood, Graybill and Boes (1974), Casella and Berger (1990), and Everitt (1998). In this paper, we use the one advocated by Everitt, that is $f_X(x) = \dfrac{b}{a^b} x^{b-1} e^{-\left(x/a\right)^b}$, since this is the same parameterization used in MATLAB®. Under this parameterization, $a > 0$ is the scale parameter and $b > 0$ is the shape parameter.
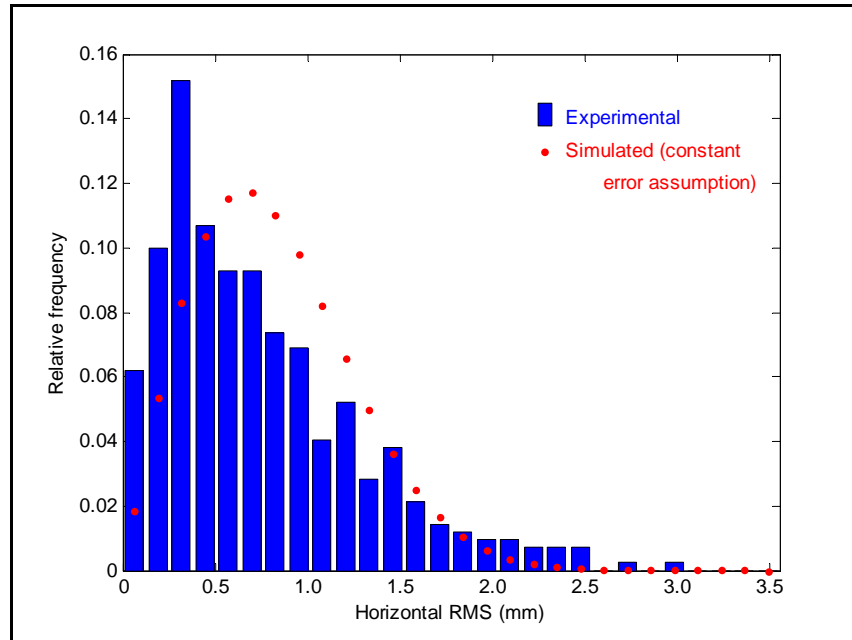
Figure 15. Comparison of relative frequency histograms of experimental RMS and simulated RMS under assumption of constant errors in the vertical directions.

It is evident in both figures 14 and 15 that the statistical model used to estimate the displacement errors is not consistent with the experimental data. In particular, the mode (i.e., the position of the peak on the abscissa) of each distribution is noticeably overestimated by the simulated distribution. The inconsistency was produced by the assumption of a constant standard deviation of the error in the projectile lateral c.g. displacements. A review of the complete set of the radiograph film shows that the images from different stations vary noticeably in clarity. Those with more sharpness and contrast could be expected to produce more accurate readings, and so it is reasonable to assume that the displacement error standard deviation behaves as a random variable. Additionally, the processor of the film could change on a shot-to-shot basis, causing the films to be much darker or lighter. Hence, we incorporated this observation into the error analysis by simulating sets of RMS values, where the ith RMS is drawn from a Weibull

distribution with *varying* scale parameter $\dfrac{\sigma_i}{\sqrt{2}}$ and shape parameter 2.

The choice of a distribution to use in modeling the displacement errors (that is, $\sigma_1, \sigma_2, \ldots, \sigma_N$) is quite subjective. In Bayesian statistical analyses, the inverted gamma distribution is frequently used as a prior distribution for variances; under this precedent, we considered the square root of an inverted gamma (RIG) distribution to model displacement errors. We also considered a gamma distribution, since this relatively simple distribution is quite versatile for modeling random variables that are right-skewed, as would be expected with displacement errors. In setting the parameters of the gamma

18

and RIG distributions – both have two parameters – we imposed the constraint that the expected value equals the maximum likelihood estimate of the displacement error under the constant error assumption.

The expected value of a RIG random variable with scale parameter a and shape parameter b can be shown to equal $\dfrac{1}{\sqrt{a}} \dfrac{\Gamma(b-1/2)}{\Gamma(b)}$ (see appendix B). Hence, we allowed b to vary while setting $a = \left[\dfrac{\Gamma(b-1/2)}{\hat{\sigma}\,\Gamma(b)}\right]^2$, and chose the RIG distribution that best matched the experimental and simulated RMS values. To objectively select a set of "best" RIG parameters, we compared the empirical cumulative distribution functions of experimental and simulated, using the maximum vertical distance between these curves as a measure of the goodness of fit, similar to a Kolmogorov-type test statistic used in nonparametric distribution fitting (see Conover, 1980). Although not shown here, even the "best" RIG distributions had a much greater likelihood of high RMS values than was observed in the experimental results.

The expected value of a gamma random variable with scale parameter a and shape parameter b is simply their product ab. Therefore, we again allowed b to vary while setting $a = \hat{\sigma}/b$, and chose the gamma distribution that yielded the best match between the experimental and simulated RMS values using the Kolmogorov vertical distance to evaluate various models.

For the horizontal data, the best gamma-distributed fit was obtained with a scale parameter of .4027 and a shape parameter of 3.25; for the vertical data, a scale parameter of 0.1684 and a shape parameter of 7.2 produced the best fit. Figures 16 and 17 show the relative frequency histograms of the experimental RMS values overlaid with the relative frequencies of values obtained through simulation with these "best fit" parameters. The gamma-distributed model horizontal RMS values still had relative frequencies that diminished at lower RMS values than observed in the experimental results, although not as severely as with the best RIG-distributed model. The RMS frequency peak locations agree noticeably better using the gamma-distributed model.

Figure 16. Comparison of relative frequency histograms of experimental RMS and simulated RMS under assumption of gamma-distributed (a=.4027, b=3.25) errors in the horizontal direction.

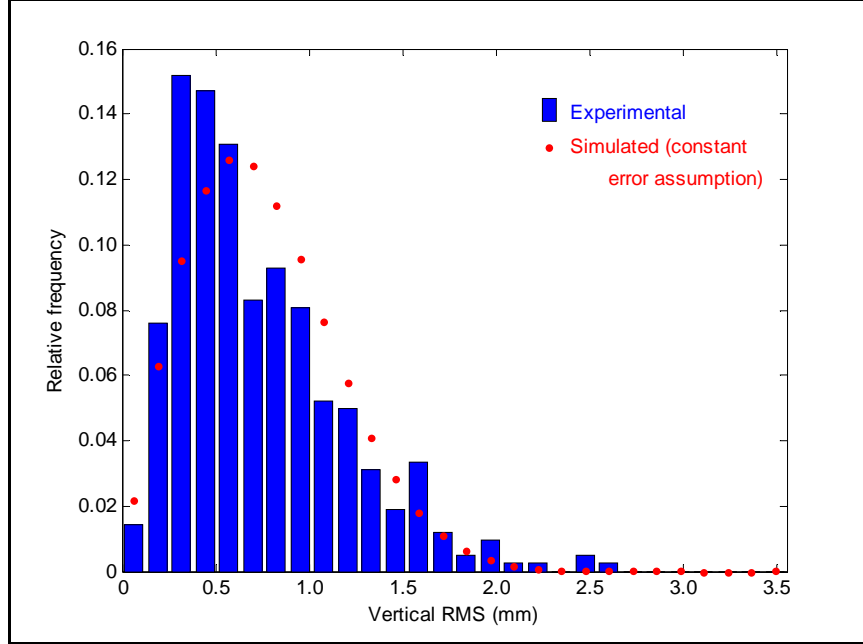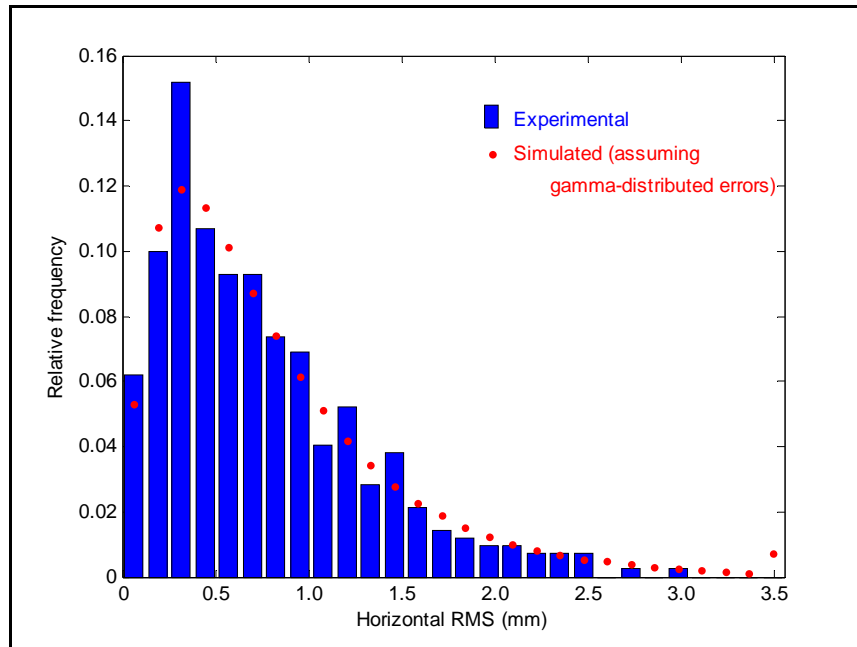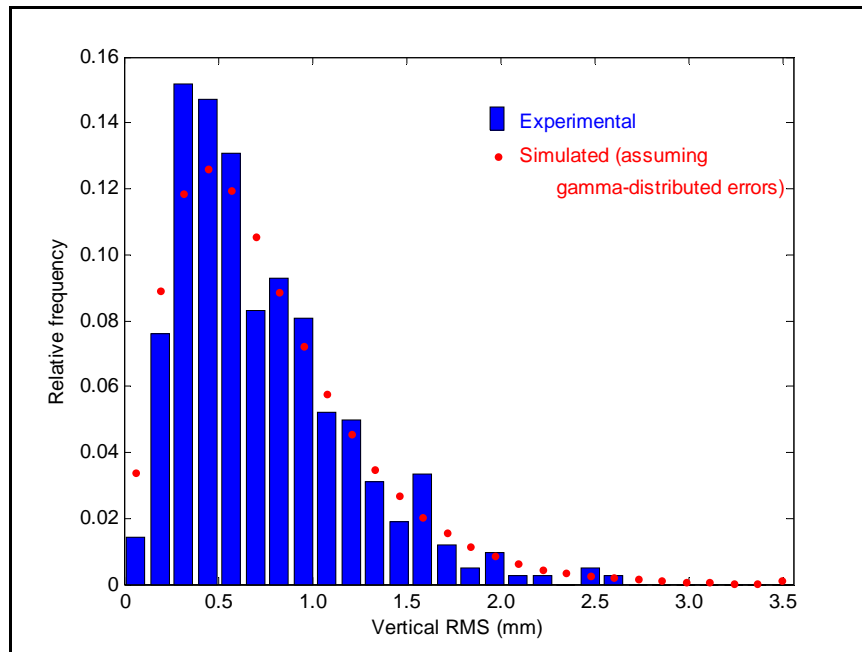Figure 17. Comparison of relative frequency histograms of experimental RMS and simulated RMS under assumption of gamma-distributed (a=.1684, b=7.2) errors in the vertical direction.

As we imposed in choosing the gamma distribution parameters, the simulated distributions produce expected standard deviation estimates in the horizontal and vertical lateral directions, $\hat{\sigma}_H$ and $\hat{\sigma}_V$, of 1.21 and 1.31 mm, respectively. For estimation purposes, we will use an approximate value of 1.25 mm. Using this estimate of the lateral displacement measurement error, the Monte Carlo simulation shows the expected standard deviation in calculated trajectory angle to be approximately 0.14 deg, as shown in figure 18.
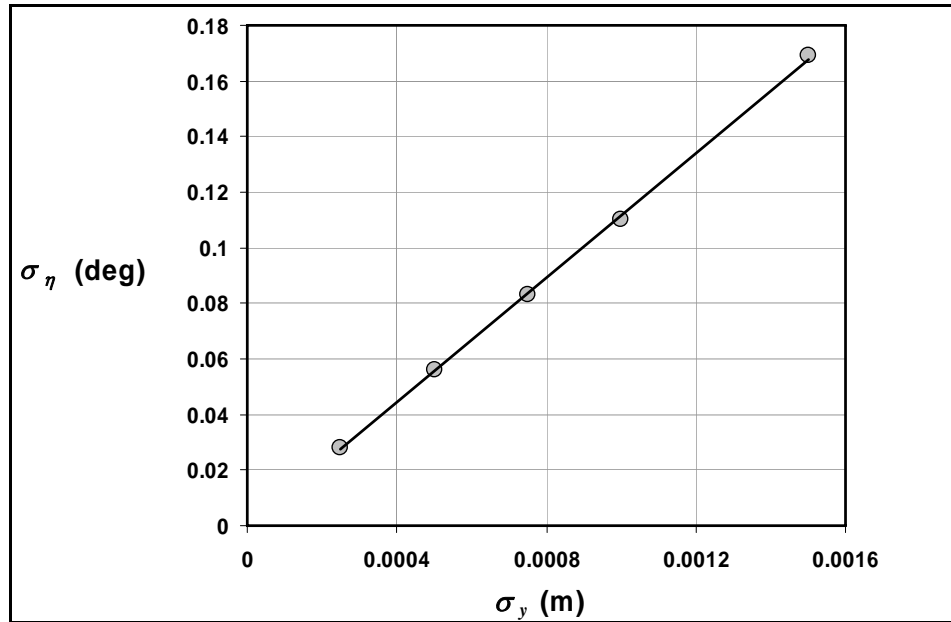
Figure 18. Estimated standard deviation of trajectory as a function of reading error.

The target impact yaw error analysis to be presented subsequently demonstrates that minimization of the trajectory angle error is an important aspect of the experiment setup. A review of the setup and consideration of the major contributors to trajectory angle error was performed, and engineering controls were considered for future implementation. The first consideration is the manner that the tube heads were aligned into the orthogonal planes. The heads were aligned using hand tools, levels and plumb bobs, and this approach provides lateral measurement accuracy to about 2 to 3 mm. Additionally, in this series of shots, the radiograph fixture was placed on a table which was leveled using shims. In an ideal setting, the fixture would have the ability to be anchored directly to the floor, by use of adjustable legs to level the fixture. The final engineering control measure would be the surveying in of the tube head and fiducial wires so the actual location of these could be known to within a single millimeter. If the exact locations of the tube heads are recorded, the digitizing program can adjust the apparent locations to the actual location more accurately. If these engineering controls are done the RMS error would be reduced significantly to only the placing of the template on the image. In effect, the film reading error would become a larger portion of the total measurement error.

4.2   Target Impact Angle Error

To estimate the error of the target impact angles, γ_T, first the projectile angular orientation measurement error, σ_α, needed to be accurately estimated. Two different methods of evaluation were completed and compared. The first method was conducted using linear aerodynamics Monte Carlo simulations of prescribed pitch and yaw motions using prescribed pitch and yaw errors. The RMS values of the simulations were then compared to those produced from the set of linear aerodynamics fits of a large number of actual shots. The second method used a statistical analysis to reproduce a histogram, via simulation, similar to the RMS values produced from the large number of actual experimental linear aerodynamic fits to estimate the error. Upon completion of the individual measurement error assessment, a Monte Carlo simulation was conducted to relate the individual measurement errors to the target impact angle error.

The linear aerodynamics Monte Carlo simulations were performed as follows. Several specific M855 motions were prescribed by specifying the six linear aerodynamic motion parameters: K_F, K_S, ϕ_{Fo}, ϕ_{So}, ϕ_F', and ϕ_S'. The M855 turning rates, ϕ_F' and ϕ_S', were prescribed to be their nominal values for each simulation. The two modal arm magnitudes, K_F and K_S, were both fixed at 2 deg. The slow arm reference orientation was prescribed to be 29 deg. The fast arm reference orientation was varied for each simulation to position the specified motion within a variety of fast arm phases. The fast arm reference orientation was found to have no noticeable effect on the results to be presented.

Next, simulated values of pitch and yaw angle were randomly generated at each of the four radiograph stations. Using the aerodynamic motion parameters: K_F, K_S, ϕ_{Fo}, ϕ_{So}, ϕ_F', and ϕ_S', as previously prescribed, allowed the calculation of the corresponding values of pitch and yaw angle at each of the four radiograph stations. Randomly generated values of pitch and yaw angle at each radiograph station were specified to be normally distributed about the calculated values, i.e., with no bias. The standard deviation error of the prescribed pitch and yaw angles, denoted σ_α, were varied for three different cases to be 0.1, 0.2, and 0.3 deg. The angle error standard deviations were assumed to be the same in the pitch and yaw planes. In each case, the randomly generated pitch and yaw angle data sets were fitted to the linear aerodynamics equations of motions using the same least squares approach used to analyze data sets from actual firings.

For each prescribed motion, the Monte Carlo simulation was performed for 1000 cases in which pitch and yaw angles were randomly generated. In each case, the RMS of the fit, comprised of the differences between the pitch and yaw angles from the prescribed and randomly generated cases, was recorded. The results of three representative simulations demonstrated an approximate match of .15 deg. Thus the Monte Carlo simulations were

22

reevaluated at five different angle error standard deviation levels of .1, .13, .15, .18, and .2 deg, and again the fit RMS error was recorded. Figure 19 depicts the RMS error for all five Monte Carlo simulations and the actual experimental RMS errors for 287 shots observed versus the relative frequency.
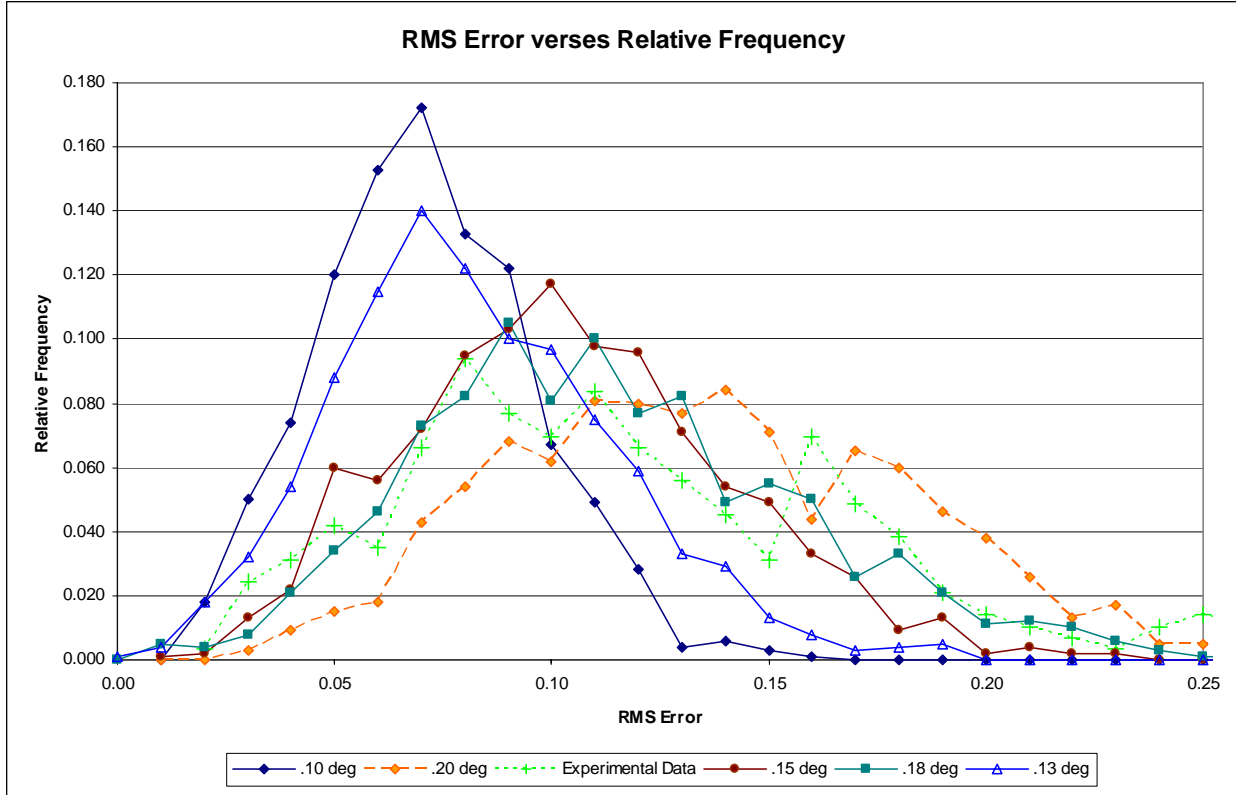
Figure 19. Least-squares fit RMS distribution from Monte Carlo simulations.

The distribution peak location for the 0.15 deg error simulation appears to be near that of the actual firings. However, the relative frequencies of the 0.15 deg error simulations appear to diminish at lower RMS values than the actual firings; the relative frequencies of the 0.20 deg error simulation appear to diminish in a manner more consistent with the actual firings. It can be speculated that the difference between the distribution shapes of the 0.15 deg error simulation and the actual firings is attributable to the difference in magnitude of yaw levels that each represents. Specifically, the simulations use a prescribed maximum yaw of 4 deg throughout. The 287 actual firings, on the other hand, include approximately 60 shots having maximum yaw levels greater than 10 deg, and several between 18 to 22 deg. These relatively high-yaw shots can be expected to have larger RMS fit values, even though the ratio of RMS value to maximum yaw level may remain constant or even decrease compared to the low yaw shots. Given these considerations, a measurement error between 0.15 and 0.20 deg is determined using the method of using linear aerodynamics Monte Carlo simulations to estimate measurement error.

The second method used to quantify the error was performed by statistically fitting the three-dimensional trajectory model RMS values to a distribution. This method lacks the theoretical basis used in the one-dimensional trajectory angle case previously discussed, because the distribution of the eight individual errors which comprise the RMS follow in the complex non-linear equation used to fit the data is unknown. However, the following analysis continues to make use of the usual regression assumption that the sum of squared deviations (observed minus predicted values) follow a chi-squared distribution. The degrees of freedom associated with this distribution are calculated as $n - p = 4$, where $n = 8$, the number of observations, and $p = 4$, the number of parameters fit in the model.

It can be shown (see appendix C) that the maximum likelihood estimator for the standard deviation of individual errors in the 3-D model, denoted by σ, is still $\hat{\sigma} = \sqrt{\dfrac{2}{N}\sum_{i=1}^{N} R_i^2}$.

Based on 287 observations, we obtained a standard deviation estimate of $\hat{\sigma} = .20$ deg. A comparison of the relative frequency histograms of 287 experimental 3-D RMS values and 500,000 simulated 3-D RMS values under the assumption of a constant standard deviation of $\hat{\sigma} = .20$ deg is displayed in figure 20. We see that the fit is poor, and so we try to fit a model in which the standard deviation is a random quantity that changes with each shot. The choice of parameters which minimized the vertical distance between the experimental and simulated RMS cumulative distribution functions was $a = .0164$ and $b = 12.25$. Simulated RMS values from this distribution have an expected standard deviation of .20 deg. the same as that obtained using the chi-squared distribution. Figure 21 compares the experimental and simulated relative frequency histograms of the 3-D RMS values when the standard deviations are modeled with this gamma distribution.
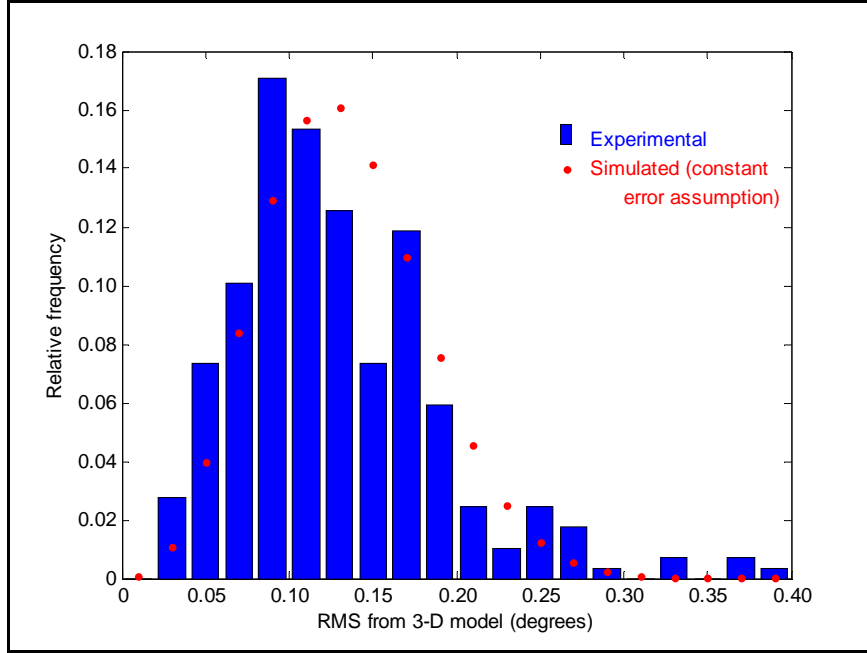
Figure 20. Comparison of relative frequency histograms of experimental RMS and simulated RMS under assumption of constant errors.
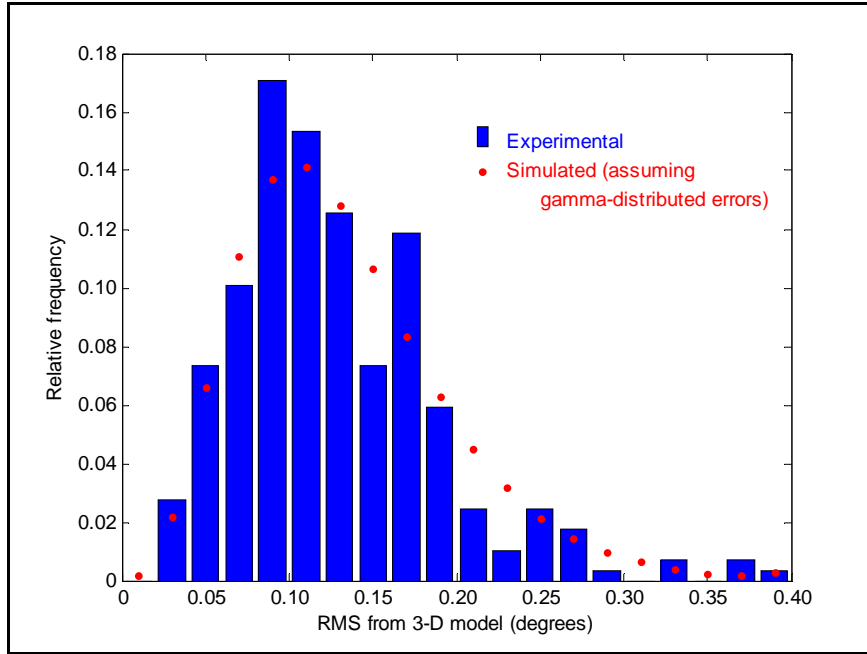
Figure 21. Comparison of relative frequency histograms of experimental RMS and simulated RMS under assumption of gamma-distributed (a=.0164, b=12.25) errors.

The linear aerodynamics Monte Carlo simulations were also used to generate target impact angle error distributions, denoted here as ε_γ, shown in figure 22. A statistical test was applied to verify that the ε_γ distributions were half-normal distributions. The estimated standard deviation centered about zero, denoted σ_γ, was calculated for each

simulation using equation 13.

$$\sigma_\gamma = \sqrt{\frac{\sum_{i=1}^{N} \varepsilon_\gamma^2}{N}} \; . \tag{13}$$

For values of σ_α of 0.1, 0.2, and 0.3 deg, the corresponding values of σ_γ were found to be 0.096, 0.192, and 0.286 deg, respectively, and graphically in figure 23. For practical purposes, the relationship is linear and σ_γ is nearly equal to σ_α for the experimental setup of this study. The fact that σ_γ is nearly equal to σ_α for the experimental setup of this study is coincidental. Certain variations in setup parameters would decrease the value of σ_γ compared to σ_α. Examples would be: (1) moving the target farther downrange from the fourth radiograph station, (2) increasing the distance between radiograph stations, and (3) using three radiograph stations instead of four. Multiple Monte Carlo simulations varying the fast mode reference value showed variations in σ_γ to be negligible.
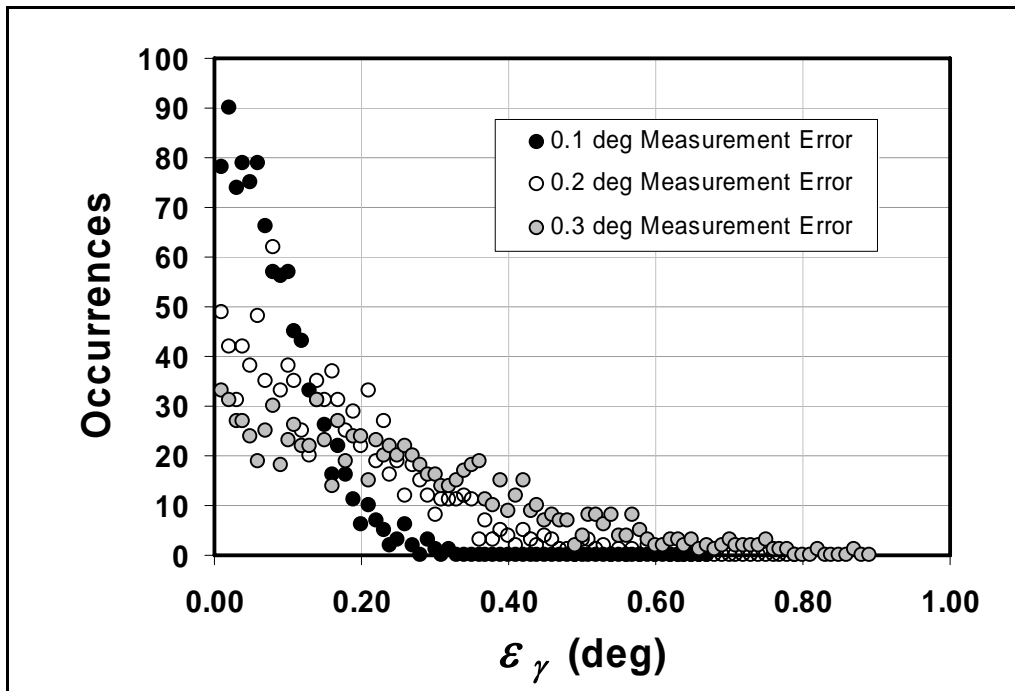
Figure 22. Monte Carlo simulation of impact yaw error distribution.
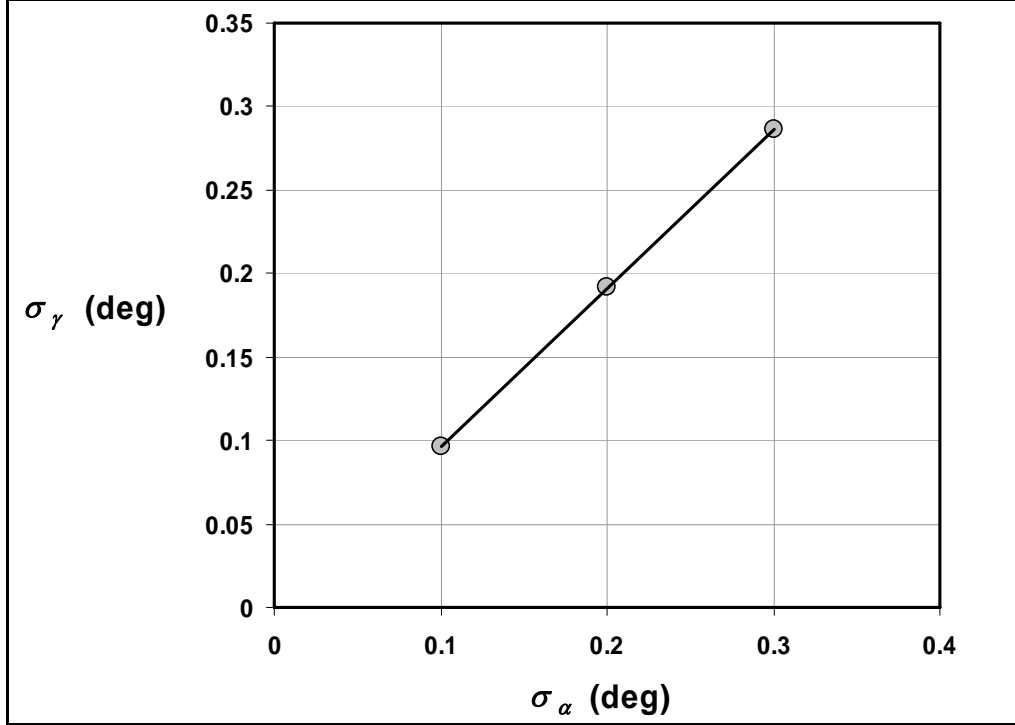
Figure 23. Estimated standard deviation of total impact yaw as a function of reading error.

The linear aerodynamics Monte Carlo simulations show the estimated projectile angle measurement error to be between 0.15 and 0.20 deg. The statistical fit shows the measurement error to be approximately 0.20 deg. Figure 23 shows that these levels of projectile measurement error correspond to a target impact angle error of approximately 0.15 to 0.20 deg.

The estimated target impact yaw error includes some influence of trajectory angle error via consideration of the RMS fit errors of the actual firings. However, the linear aerodynamics model does not include this effect, which is manifested as a shot-to-shot bias in the assumed origin of the pitch versus yaw coordinate system. That is, the origin of the pitch and yaw data for a particular shot is expected to be shifted by the estimated trajectory angle error, 0.14 deg. The effect of this biased trajectory angle measurement error on the target impact yaw error can be conservatively estimated by calculating an adjusted target impact yaw error, σ'_γ, i.e.,

$$\sigma'_\gamma = \sqrt{\sigma_\gamma^2 + \sigma_\eta^2} \,, \tag{14}$$

in which no correlation is assumed to exist between σ_γ and σ_η. For $\sigma_\eta = 0.14$ deg and $\sigma_\gamma = 0.15$ deg, σ'_γ is calculated to be approximately 0.21 deg. For $\sigma_\eta = 0.14$ deg and $\sigma_\gamma = 0.2$ deg, σ'_γ is calculated to be approximately 0.24 deg.

5. Conclusions

At the time of this writing, approximately 500 firings had been conducted and subsequently analyzed using the Yaw at Impact program described in this report. The radiograph measurement technique and the linear aerodynamics model provide a cost effective and efficient approach to study the necessarily large sample sizes required to characterize the terminal ballistics of this class of small-caliber ammunition.

The study demonstrated two major benefits. First, the approach provides a means to accurately relocate the gun to a yaw node (i.e., minimum yaw), a maximum yaw location, or somewhere in between. Second, any dataset could contribute to a fleet yaw characterization because a reduction for each shot yields values of the fast and slow modal arms, K_f and K_s, whose sum is the maximum yaw. This would provide an alternative to fleet yaw characterization in the spark range after the initial aerodynamics characterization is completed.

Error estimation was an important aspect of the current effort. Error levels were estimated by relating the RMS values of fitted trajectory parameters to those generated using statistical simulations. By doing so, the estimated measurement errors of the projectile lateral displacement and angular orientation data points could be obtained. These error levels were directly related to the trajectory angle and impact angle errors. For the current set of firings, the estimated error of the projectile trajectory angle (that is the velocity vector orientation relative to the fiducial wire) was found to be approximately 0.14 deg. The estimated error of the target impact angle using linear aerodynamics theory was found to be between 0.15 and 0.20 deg. If the trajectory angle error is considered a bias in the system, then the target impact angle error would be between 0.21 and 0.24 deg.

A review of the experiment setup was made and possible improvements were suggested. Most significant perhaps is that the error estimation methodology provides a basis for evaluating alternative radiograph setup parameters. The approach is a useful tool for designing an experimental setup that can minimize error within the spatial constraints usually associated with radiograph equipment and instrumentation. At the very least, such considerations could prevent the use of experimental parameters that could create larger errors than were estimated in the current study.

References

Casella, G.; Berger, R. L. *Statistical Inference*, 2nd ed., Duxbury Press: Belmont, CA, 1990.

Conover, W. J. *Practical Nonparametric Statistics*, 2nd ed., John Wiley & Sons: New York, 1980.

Everitt, B. S. *The Cambridge Dictionary of Statistics*, Cambridge University: Cambridge, U.K., 1998.

McCoy, R.L. *Aerodynamic and Flight Dynamic Characteristics of the New Family of 5.56 mm NATO Ammunition*; BRL-MR-3476; U.S. Army Ballistic Research Laboratory: Aberdeen Proving Ground, MD, October 1985.

McCoy, R.L. *Modern Exterior Ballistics*, Schiffer Publishing Ltd.: Atglen, PA, 1998.

Mood, A.; Graybill, F.; Boes, D. *Introduction to the Theory of Statistics*, 3rd ed., McGraw-Hill: New York, 1974.

Zook, J.A.; Frank, K; Silsby, G.F. *Terminal Ballistics Test and Analysis Guidelines for the Penetration Mechanics Branch*; BRL-MR-3960; U.S. Army Ballistic Research Laboratory: Aberdeen Proving Ground, MD, January 1992.

INTENTIONALLY LEFT BLANK.

Appendix A: Maximum Likelihood Estimation of the Displacement Standard Deviation

To derive a maximum likelihood estimator for the displacement standard deviation, σ, from a set of RMS values it is necessary to know their probability density function. It is well established that $\dfrac{\sum_{j=1}^{4}\left(d_{ij}-\hat{d}_{ij}\right)^2}{\sigma^2}$ is distributed as a chi-square random variable with two degrees of freedom. Therefore $S=\dfrac{1}{\sigma}\sqrt{\sum_{j=1}^{4}\left(d_{ij}-\hat{d}_{ij}\right)^2}=\dfrac{2}{\sigma}R_i$ is a chi random variable with two degrees of freedom, having the probability density function $f_S(s)=se^{-\left(s^2/2\right)}$ for $s>0$. This is also the probability density function of a Weibull random variable with scale parameter $\sqrt{2}$ and shape parameter 2.

To derive the probability density function of R, we write $R=g(S)=\dfrac{\sigma}{2}S$, noting that $\sigma>0$. Following the methods described in Chapter 5, Section 5 of Mood, Graybill, and Boes (1974), the probability density function of R is given by

$$
\begin{aligned}
f_R(r) &= \left|\frac{d}{dr}g^{-1}(r)\right|f_S\left(g^{-1}(r)\right) \\[6pt]
&= \left|\frac{d}{dr}\frac{2r}{\sigma}\right|f_S\left(\frac{2r}{\sigma}\right) \\[6pt]
&= \frac{2}{\sigma}\left(\frac{2r}{\sigma}\right)e^{-\left(\frac{2r}{\sigma}\right)^2/2} \\[6pt]
&= \frac{4r}{\sigma^2}e^{-2r^2/\sigma^2}
\end{aligned}
\tag{A-1}
$$

for $r>0$. This is the probability density function of a Weibull random variable with scale parameter $\dfrac{\sigma}{\sqrt{2}}$ and shape parameter 2.

Now suppose that a random sample of N RMS values is drawn from the Weibull distribution with scale parameter $\dfrac{\sigma}{\sqrt{2}}$ and shape parameter 2. The likelihood function is

$$L(\sigma) = \prod_{i=1}^{N} \frac{4r_i}{\sigma^2} e^{-2r_i^2 / \sigma^2} = \frac{4^N}{\sigma^{2N}} e^{-\frac{2}{\sigma^2}\sum_{i=1}^{N} r_i^2} \prod_{i=1}^{N} r_i , \qquad (A\text{-}2)$$

and the log-likelihood is

$$\ln L(\sigma) = N \ln 4 - 2N \ln \sigma - \frac{2}{\sigma^2} \sum_{i=1}^{N} r_i^2 + \sum_{i=1}^{N} \ln(r_i) \qquad (A\text{-}3)$$

taking the derivative with respect to σ,

$$\frac{d}{d\sigma} \ln L(\sigma) = -2N \frac{1}{\sigma} - 2\sum_{i=1}^{N} r_i^2 \left(\frac{-2}{\sigma^3}\right) = \frac{-2N}{\sigma} + \frac{4\sum_{i=1}^{N} r_i^2}{\sigma^3} . \qquad (A\text{-}4)$$

Setting this last expression to zero and solving for σ one gets,

$$0 = \frac{-2N}{\hat{\sigma}} + \frac{4\sum_{i=1}^{N} r_i^2}{\hat{\sigma}^3} \quad \Leftrightarrow \quad 2N = \frac{4\sum_{i=1}^{N} r_i^2}{\hat{\sigma}^2} \quad \Leftrightarrow \quad \hat{\sigma} = \sqrt{\frac{2}{N} \sum_{i=1}^{N} r_i^2} . \qquad (A\text{-}5)$$

So the maximum likelihood estimator for the displacement standard deviation, σ, is given by

$$\hat{\sigma} = \sqrt{\frac{2}{N} \sum_{i=1}^{N} r_i^2} . \qquad (A\text{-}6)$$

Appendix B: Expected Value of the Square Root of an Inverted Gamma Random Variable

To derive the expected value of a random variable that is the square root of an inverted gamma (RIG) random variable, its probability density function is first needed. First, let X be a gamma distributed random variable with scale parameter a and shape parameter b. Then the probability density function of X is

$$f_X(x) = \frac{1}{a^b \Gamma(b)} x^{b-1} e^{-x/a}. \qquad (B-1)$$

Then $Y = g(X) = \sqrt{1/X}$ is a RIG random variable with density

$$\begin{aligned}
f_Y(y) &= \left| \frac{d}{dy} g^{-1}(y) \right| f_X\left(g^{-1}(y)\right) \\
&= \left| \frac{d}{dy}\left(\frac{1}{y^2}\right) \right| \frac{1}{a^b \Gamma(b)} \left(\frac{1}{y^2}\right)^{b-1} e^{-\left(\frac{1}{y^2}\right)/a} \\
&= \left| -2y^{-3} \right| \frac{1}{a^b \Gamma(b)} y^{-2(b-1)} e^{-1/ay^2} \\
&= \frac{2}{a^b \Gamma(b)} y^{-2(b-1)-3} e^{-1/ay^2} \\
&= \frac{2}{a^b \Gamma(b)} y^{-2b-1} e^{-1/ay^2}
\end{aligned} \qquad (B-2)$$

The expected value of Y is

$$\begin{aligned}
E(Y) &= \int y f_Y(y) dy \\
&= \int_0^\infty y \frac{2}{a^b \Gamma(b)} y^{-2b-1} e^{-1/ay^2} dy. \\
&= \frac{2}{a^b \Gamma(b)} \int_0^\infty y^{-2b} e^{-1/ay^2} dy
\end{aligned} \qquad (B-3)$$

33

Now let $z = y^{-1}$. Then $y = z^{-1}$ and $dy = -z^{-2}dz$. Making a change of variable inside the integral, we have,

$$E(Y) = \frac{2}{a^b \Gamma(b)} \int_{\infty}^{0} z^{2b} e^{-z^2/a} \left(-z^{-2}dz\right)$$

$$= \frac{2}{a^b \Gamma(b)} \int_{0}^{\infty} z^{2b-2} e^{-z^2/a} \, dz$$

$$= \frac{2}{a^b \Gamma(b)} \int_{0}^{\infty} z^{2b-3} z e^{-z^2/a} \, dz \qquad . \qquad \text{(B-4)}$$

$$= \frac{2}{a^b \Gamma(b)} \frac{b}{2} \int_{0}^{\infty} z^{2b-3} \frac{2}{a} z e^{-z^2/a} \, dz$$

$$= \frac{1}{a^{b-1}\Gamma(b)} \int_{0}^{\infty} z^{2b-3} \frac{2}{\sqrt{a}^2} z e^{-\left(z/\sqrt{a}\right)^2} \, dz$$

Notice that the expression $\dfrac{2}{\sqrt{a}^2} z e^{-\left(z/\sqrt{a}\right)^2}$ within the integrand is the probability density function of a Weibull random variable with scale parameter $\sqrt{a}$ and shape parameter 2. Without loss of generality, we can temporarily refer to this random variable as T. This facilitates us in recognizing the integral as the $(2b-3)^{th}$ raw moment of T. That is,

$$E(Y) = \frac{1}{a^{b-1}\Gamma(b)} \int_{0}^{\infty} t^{2b-3} \frac{2}{\sqrt{a}^2} z e^{-\left(z/\sqrt{a}\right)^2} \, dt$$

$$= \frac{1}{a^{b-1}\Gamma(b)} E\left(T^{2b-3}\right) \qquad . \qquad \text{(B-5)}$$

$$= \frac{1}{a^{b-1}\Gamma(b)} \left[\sqrt{a}^{\,2b-3} \Gamma\left(1 + \frac{2b-3}{2}\right)\right]$$

Simplification of this final expression yields

$$E(Y) = \frac{1}{\sqrt{a}} \frac{\Gamma\left(b - \frac{1}{2}\right)}{\Gamma(b)} . \qquad \text{(B-6)}$$

Appendix C: Maximum Likelihood Estimation of the Three Dimensional Displacement Standard Deviation

To derive a maximum likelihood estimator for the 3-D displacement standard deviation, σ, from a set of RMS values it is necessary to know the probability density function of these RMS values. We assume that $D_i = \dfrac{\sum\limits_{j=1}^{8}\left(d_{ij} - \hat{d}_{ij}\right)^2}{\sigma^2}$ is distributed as a chi-square random variable with four degrees of freedom. Therefore,

$$\sqrt{D_i} = \sqrt{\frac{\sum\limits_{j=1}^{8}\left(d_{ij} - \hat{d}_{ij}\right)^2}{\sigma^2}} = \frac{\sqrt{8}}{\sigma}\sqrt{\frac{1}{8}\sum\limits_{j=1}^{8}\left(d_{ij} - \hat{d}_{ij}\right)^2} = \frac{\sqrt{8}}{\sigma}R_i = S_i \qquad \text{(C-1)}$$

is a chi random variable with four degrees of freedom, having the probability density function $f_S(s) = \dfrac{1}{2}s^3 e^{-s^2/2}$ for $s > 0$.

If we let $R = g(S) = \dfrac{\sigma}{\sqrt{8}}S$, the probability density function of R is given by

$$\begin{aligned}
f_{R_i}(r) &= \left|\frac{d}{dr}g^{-1}(r)\right| f_S\left(g^{-1}(r)\right) \\
&= \left|\frac{d}{dr}\frac{\sqrt{8}}{\sigma}r\right| f_S\left(\frac{\sqrt{8}}{\sigma}r\right) \\
&= \frac{\sqrt{8}}{\sigma}\frac{1}{2}\left(\frac{\sqrt{8}}{\sigma}r\right)^3 e^{-\left(\frac{\sqrt{8}}{\sigma}r\right)^2/2} \\
&= \frac{32}{\sigma^4}r^3 e^{-4r^2/\sigma^2}
\end{aligned} \qquad \text{(C-2)}$$

for $r > 0$. This density function does not match any of the commonly used distributions.

Now suppose that a random sample of N RMS values is drawn. The likelihood function is

$$L(\sigma) = \prod_{i=1}^{N}\frac{32}{\sigma^4}r_i^3 e^{-4r_i^2/\sigma^2} = \frac{32^N}{\sigma^{4N}}e^{-\frac{4}{\sigma^2}\sum\limits_{i=1}^{N}r_i^2}\prod_{i=1}^{N}r_i^3, \qquad \text{(C-3)}$$

And the log-likelihood is

$$\ln L(\sigma) = N \ln 32 - 4N \ln \sigma - \frac{4}{\sigma^2} \sum_{i=1}^{N} r_i^2 + \sum_{i=1}^{N} \ln(r_i^3). \qquad \text{(C-4)}$$

Taking the derivative with respect to σ,

$$\frac{d}{d\sigma} \ln L(\sigma) = -4N \frac{1}{\sigma} - 4 \sum_{i=1}^{N} r_i^2 \left(\frac{-2}{\sigma^3} \right) = \frac{-4N}{\sigma} + \frac{8 \sum_{i=1}^{N} r_i^2}{\sigma^3}. \qquad \text{(C-5)}$$

Setting this last expression to zero and solving for σ one gets,

$$0 = \frac{-4N}{\hat{\sigma}} + \frac{8 \sum_{i=1}^{N} r_i^2}{\hat{\sigma}^3} \quad \Leftrightarrow \quad 4N = \frac{8 \sum_{i=1}^{N} r_i^2}{\hat{\sigma}^2} \quad \Leftrightarrow \quad \hat{\sigma} = \sqrt{\frac{2}{N} \sum_{i=1}^{N} r_i^2}. \qquad \text{(C-6)}$$

So the maximum likelihood estimator for the displacement standard deviation, σ, is given by

$$\hat{\sigma} = \sqrt{\frac{2}{N} \sum_{i=1}^{N} r_i^2}. \qquad \text{(C-7)}$$

Abbreviations and Symbols

C_{M_α}	pitching moment coefficient
K-factor	Magnification factor
K_F	Fast modal arm magnitude
K_S	Slow modal arm magnitude
x	downrange location of projectile
x_0	the designated downrange location of projectile where x = 0
R	Root Mean Square (RMS)
a	scale parameter of either a gamma or Weibull distribution function
b	shape parameter of either a gamma or Weibull distribution function

Greek Symbols

α	pitch angle
β	yaw angle
γ	total angle
η	trajectory
α_A and β_A	apparent pitch and yaw
α_C and β_C	corrected pitch and yaw
α_T and β_T	pitch and yaw at target
γ_T	total angle at target
$\tilde{\xi}$	complex angle of attack
α_{Cen} and β_{Cen}	fast arm pitch and yaw center
ϕ_{Fo}	reference phase angle of the fast epicyclic modal arm, evaluated at $x = x_0$ and real

ϕ_{So}	reference phase angle of the slow epicyclic modal arm, evaluated at x= x_0 and real
ϕ'_F	turning rate of the fast epicyclic modal arm, real
ϕ'_S	turning rate of the slow epicyclic modal arm, real
σ_α	standard deviation of reading error
σ_γ	standard deviation of error at target
ε_α & ε_β	error for each station; difference between the α_C and β_C angles obtained from the radiographs and those obtained from the linear aerodynamics free-flight equations of motion
ε_γ	error on target caused by measurement error of radiographs
σ	standard deviation
$\hat{\sigma}$	estimate of standard deviation
$\Gamma(x)$	gamma function evaluated at x

Distribution List

No. of Copies	Organization	No. of Copies	Organization
1 CD	US ARMY RESEARCH LAB ATTN IMNE ALC IMS MAIL & RECORDS MGMT ADELPHI MD 20783-1197	5 HC	ATK ROLLIE DOHRN MN07 LW54 CRAIG AAKHUS MN07 LW54 MARK JANTSCHER MN07 LW54 DIPAK KAMDAR MN07 LW54 BOB BECKER MN07 MW44 5050 LINCOLN DR EDINA MN 55436
1 ELEC	ADMNSTR DEFNS TECHL INFO CTR ATTN DTIC OCP V MADDOX 8725 JOHN J KINGMAN RD STE 0944 FT BELVOIR VA 22060-6218	1 HC	ATK LAKE CITY KEITH ENLOW PO BOX 1000 INDEPENDENCE MO 64051-1000
2 CDS	US ARMY RESEARCH LAB AMSRD ARL CI OK TL TECHL LIB 2800 POWDER MILL ROAD ADELPHI MD 20783-1197	7 HC	ATK LAKE CITY SMALL CALIBER AMMUNITION LAKE CITY ARMY AMMUNITION PLANT DAN MANSFIELD (5 COPIES) JOHN WESTBROOK MO10 003 PO BOX 1000 INDEPENDENCE MO 64051-1000
1 ELEC	US ARMY RESEARCH LAB AMSRD CI OK TP TECHL LIB APG MD 21005		
1 HC	PRODUCT MANAGER SMALL AND MEDIUM CALIBER AMMO SFAE AMO MAS SMC LTC FLETCHER BLDG 354 PICATINNY ARSENAL NJ 07806-5000	1 HC	US ARMY TACOM ARDEC CCAC AMSTA AR CCL C GARY FLEMING BLDG 65N PICATINNY ARSENAL NJ 07806-5000
5 HC	APM SMALL & MEDIUM CALIBER AMMO SFAE AMO MAS SMC ROBERT KOWALSKI MAJ LAFONTAINE FRANK HANZL PAUL RIGGS GREGORY DEROSA BLDG 354 PICATINNY ARSENAL NJ 07806-5000	1 HC	US ARMY TACOM ARDEC CCAC AMSTA AR CCL B JOHN MIDDLETON BLDG 65N PICATINNY ARSENAL NJ 07806-5000
		1 HC	US ARMY TACOM ARDEC ASIC PROGRAM INTEGRATION OFFICE JOHN A RESCH BLDG 1 PICATINNY ARSENAL NJ 07801

No. of Copies	Organization	No. of Copies	Organization
1 HC	US ARMY TACOM ARDEC AMSTA AR CCL B MARK D MINISI BLDG 65S PICATINNY ARSENAL NJ 07806-5000	1 HC	US ARMY TACOM ARDEC AMSTA AR AET A ANTHONY P FARINA BLDG 95 PICATINNY ARSENAL NJ 07806-5000
2 HC	US ARMY TACOM ARDEC SHAWN SPICKERT FULTON CHAD SENSENIG BLDG 65N PICATINNY ARSENAL NJ 07806-5000	1 HC	US ARMY TACOM ARDEC CCAC AMSRD AAR AEM I DENNIS J CONWAY BLDG 65N PICATINNY ARSENAL NJ 07806-5000
1 HC	US ARMY TACOM ARDEC AMSRD AAR AEM T MARK NICOLICH BLDG 65S PICATINNY ARSENAL NJ 07806-5000	1 HC	US ARMY TACOM ARDEC AMSTA AR FSF T HANK HUDGINS BLDG 382 PICATINNY ARSENAL NJ 07806-5000
2 HC	US ARMY TACOM ARDEC AMSRD AAR AEM SAIF J MUSALLI AMSRD AAR AEM L ERNIE LOGSDON BLDG 65S PICATINNY ARSENAL NJ 07806-5000	1 HC	SIERRA BULLETS PATRICK DALY 1400 WEST HENRY STREET SEDALIA MO 65302-0818
1 HC	US ARMY TACOM ARDEC AMSRD AAR AEM I RALPH MAZESKI BLDG 65N PICATINNY ARSENAL NJ 07806-5000	1 HC	ST MARKS POWDER GENERAL DYNAMICS ROBERT PULVER 7121 COASTAL HIGHWAY CRAWFORDVILLE FL 32327
1 HC	COMMANDER US ARMY ARDEC FIRING TABLES AND BALLISTICS DIVISION AMSRD AAR AEF T BARBARA TILGHMAN 2201 ABERDEEN BOULEVARD ABERDEEN PROVING GROUND MD 21005-5001	1 HC	ST MARKS POWDER GENERAL DYNAMICS JOHNATHAN HOWARD 7121 COASTAL HIGHWAY CRAWFORDVILLE FL 32327
1 HC	COMMANDER US ARMY ARDEC FIRING TABLES AND BALLISTICS DIVISION ATTN AMSRD AAR AEF T FRAN MIRABELLE 2201 ABERDEEN BOULEVARD ABERDEEN PROVING GROUND MD 21005-5001	3 HC	RADFORD ARMY AMMUNITION PLANT KELLY BROWN WJ WORRELL HAYES ZIEGLER PO BOX 1 ROUTE 114 RADFORD VA 24143

No. of Copies	Organization	No. of Copies	Organization
1 HC	US ARMY RSRCH LAB AMSRD ALR CI CT B BODT APG MD 21005-5067	4 HC	US ARMY RSRCH LAB AMSRL WM BD A BRANT B FORCH M NUSCA T WILLIAMS BLDG 390 APG MD 21005
1 HC	US ARMY RSRCH LAB AMSRL WM B M ZOLTOSKI BLDG 4600 APG MD 21005		
		3 HC	US ARMY RSRCH LAB AMSRL WM BF W OBERLE R PEARSON S WILKERSON BLDG 390 APG MD 21005
1 HC	US ARMY RSRCH LAB AMSRL WM BA D LYON BLDG 4600 APG MD 21005		
		1 HC	US ARMY RSRCH LAB AMSRL WM T COL ALTHOUSE BLDG 309 APG MD 21005
16 HC	US ARMY RSRCH LAB AMSRL WM BC M BUNDY J DESPIRITO I CELMINS BERNARD J GUIDOS (3 COPIES) J GARNER K HEAVEY J NEWILL P PLOSTINS J SAHU S SILTON DAVID W WEBB (3 COPIES) P WEINACHT BLDG 390 APG MD 21005	4 HC	US ARMY RSRCH LAB AMSRL WM TA M S BURKINS D HACKBARTH D SCHALL S SCHOENFELD BLDG 309 APG MD 21005
		6 HC	US ARMY RSRCH LAB AMSRD ARL WM TB TOM ADKINS RACHEL EHLERS BRIAN K KRZEWINSKI BRENDAN MCANDREW JAY TALSMA ERIC WILSON RANGE 20 APG MD 21005
4 HC	US ARMY RSRCH LAB AMSRD ARL SL BD R GROTE R KANE R KINSLER J POLESNE RANGE 20 APG MD 21005		

No. of
Copies   **Organization**

16 HC   US ARMY RSRCH LAB
           AMSRL WM TC
           J ANGLE
           R COATES
           D DIEHL
           TYLER E EHLERS (3 COPIES)
           T FARRAND
           E KENNEDY
           J KOONTZ
           L MAGNESS
           B PETERSON
           R PHILLABAUM
           B SORENSEN
           R SUMMERS
           A TANK
           G WATT
           BLDG 309
           APG MD 21005

TOTALS: 97 Hard Copies, 3 CDs, 2 Elec.